UNCLASSIFIED

AD NUMBER
ADA995208
CLASSIFICATION CHANGES

TO:	UNCLASSIFIED
FROM:	SECRET

LIMITATION CHANGES

TO:

Approved for public release; distribution is unlimited. Document partially illegible.

FROM:

Distribution authorized to U.S. Gov't. agencies only; Test and Evaluation; APR 1954. Other requests shall be referred to Air Force Cambridge Research Center, Geophysics Research Directorate, Terrestrial Science Laboratoroy, Hanscom AFB, MA. Document partially illegible.

AUTHORITY

23 Feb 1960, per document marking; afcrl, 5 Jul 1984

THIS PAGE IS UNCLASSIFIED

PHOTOGRAPH THIS SHEET

LEVEL

INVENTORY

WT-715

DOCUMENT IDENTIFICATION

Apr'54

DISTRIBUTION STATEMENT

AD A995208

DTIC ACCESSION NUMBER

ACCESSION FOR
NTIS   GRA&I
DTIC   TAB
UNANNOUNCED
JUSTIFICATION

BY
DISTRIBUTION /
AVAILABILITY CODES
DIST   AVAIL AND/OR SPECIAL

P/I

Released

D&IO
COPY
INSPECTED
2

DISTRIBUTION STAMP

UNANNOUNCED

DTIC
SELECTED
JUL 5 1984
D
D

DATE ACCESSIONED

DATE RETURNED

84 07 05 00 5

DATE RECEIVED IN DTIC

REGISTERED OR CERTIFIED NO.

PHOTOGRAPH THIS SHEET AND RETURN TO DTIC-DDAC

DTIC FORM 70A
DEC 83

DOCUMENT PROCESSING SHEET

PREVIOUS EDITION MAY BE USED UNTIL
STOCK IS EXHAUSTED.

DISCLAIMER NOTICE
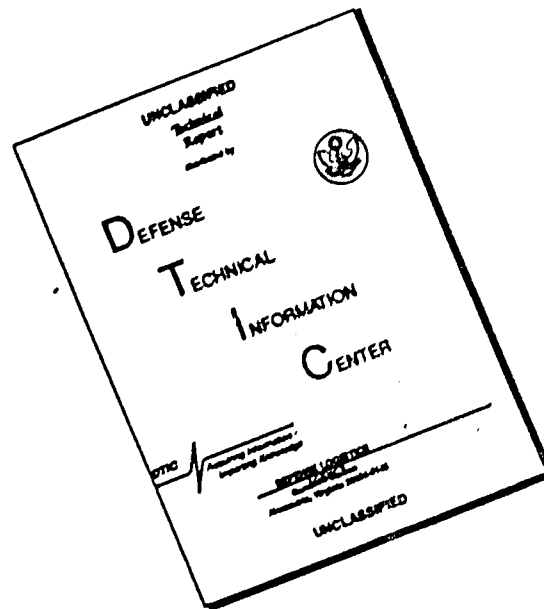
THIS DOCUMENT IS BEST QUALITY AVAILABLE. THE COPY FURNISHED TO DTIC CONTAINED A SIGNIFICANT NUMBER OF PAGES WHICH DO NOT REPRODUCE LEGIBLY.

OPERATION UPSHOT-KNOTHOLE

Project 1.3

FREE-AIR ATOMIC BLAST PRESSURE MEASUREMENTS

REPORT TO THE TEST DIRECTOR

by

Norman A. Haskell
and
Richard M. Brubaker, Major, USAF

April 1954

Terrestrial Sciences Laboratory
Geophysics Research Directorate
Air Force Cambridge Research Center

ABSTRACT

The project was designed to: (1) determine the free-air peak over-pressure vs. distance curve for air burst atomic bombs at overpressure below those covered by existing data, (2) determine the path of the triple point at high altitudes for at least one shot, (3) measure the relative strengths of the free-air and reflected shocks above the triple point and of the Mach shock below the triple point.

The project participated in Shots 4 and 9 because the points of detonation were of sufficient height above terrain to give a good separation of direct and reflected shocks over a wide range of distances. The operation was accomplished by deploying 14 parachute-borne canisters in Shot 4 (6 April) and 20 canisters in Shot 9 (8 May). Two B-29s were used in laying down each array. The preliminary positioning of the canisters was determined so as to meet the objectives stated above and the positions and times of canister release were adjusted to attain these positions at shock arrival time with allowance for wind drift during time of fall.

Each canister contained an altimeter transducer, two differential pressure transducers, and a radiotelemetry transmitter. The telemetered pressure and altimeter data were recorded at a ground station.

Complete data were received from all canisters in both tests. In Shot 4 all canisters were in the region of regular reflection. In Shot 9 14 canisters were in the region of regular reflection and 6 were in the Mach region. In addition to the main direct and reflected shocks, a small secondary shock and its ground reflection were received at nearly all canisters on Shot 9.

The free-air values have been normalized to 1 KT in a homogeneous sea-level atmosphere and used to extend the TUMBLER composite free-air curve down to overpressures of about 0.07 psi. A comparison of this curve with the results of previous tests at low heights of burst has been made to determine the effective reflection factor for these earlier shots. The path of the triple point has been determined for Shot 9 over the range of altitudes between 6500 and 10,500 ft and some tentative conclusions have been reached on the distribution of peak over-pressures in the reflected and Mach shocks in the neighborhood of the triple point.

3

FOREWORD

This report is one of the reports presenting the results of the 78 projects participating in the Military Effects Tests Program of Operation UPSHOT-KNOTHOLE, which included 11 test detonations. For readers interested in other pertinent test information, reference is made to WT-782, Summary Report of the Technical Director, Military Effects Program. This summary report includes the following information of possible general interest.

    a. An over-all description of each detonation, including yield, height of burst, ground zero location, time of detonation, ambient atmospheric conditions at detonation, etc., for the 11 shots.

    b. Compilation and correlation of all project results on the basic measurements of blast and shock, thermal radiation, and nuclear radiation.

    c. Compilation and correlation of the various project results on weapons effects.

    d. A summary of each project, including objectives and results.

    e. A complete listing of all reports covering the Military Effects Tests Program.

CONTENTS

ILLUSTRATIONS

UNCLASSIFIED

TABLES

CHAPTER 1

INTRODUCTION

1.1 OBJECTIVE

The primary objective of this project was to obtain data on the peak overpressure in the free-air shock wave from an atomic detonation before the arrival of the ground reflected wave. Measurements were particularly desired in the range of overpressures from about 8 to 0.25 psi in order to extend the measurements made by the shock velocity method at higher overpressures down to the range of interest in connection with the establishment of lethal and safe envelopes for aircraft in the vicinity of an atomic explosion.

Secondary objectives were to determine the form of the free-air pressure pulse, to establish the path of the triple point at high altitudes, and to measure the peak overpressures of the reflected and Mach shocks.

1.2 BACKGROUND

The military requirement for an operational test of the Fuchs theory relative to the blast wave in an inhomogeneous atmosphere was undertaken by the Terrestrial Sciences Laboratory, Air Force Cambridge Research Center (AFCRC), in early 1950. Following development of instruments and techniques, actual tests were conducted at Operations JANGLE, SNAPPER, and IVY. The JANGLE project was principally designed to check out instrumentation and techniques. At SNAPPER peak overpressure measurements were made over a wide range of distances and altitudes and it was shown that the variation with altitude was consistent with that deduced from the Fuchs scaling law. The results obtained at IVY, although roughly consistent with the SNAPPER data, did not cover a sufficiently large range of altitudes to provide an unambiguous test of the applicability of Fuchs scaling to weapons of very large yield.

In all of these tests the shots were either surface bursts or fired at a low scaled height and, with the exception of three measurements at King shot of IVY, all measurements were made in the region of Mach reflection. It was therefore not possible to deduce the equivalent free-air values without introducing questionable assumptions with regard to ground reflectivity. Since it is primarily the free-air peak overpressure that is desired for the computation of blast effects on aircraft, additional measurements with a high air burst were required.

CHAPTER 2

EXPERIMENT DESIGN

2.1 MEANS OF FULFILLING THE OBJECTIVE

Arrays of parachute-borne instrumented canisters were deployed
from two aircraft. The planned positions are shown in Figs. 2.1 and
2.2. The planes of the arrays were offset from ground zero, but in the
figures the canister positions are plotted at true horizontal distance
and slant range regardless of azimuth. Ambient pressure and overpres-
sure data were telemetered continuously from the canisters to a ground
recording station. In SNAPPER it was established by independent posi-
tion measurements using an electronic multiple object tracking system
(MOTS) that slant ranges could be computed from shock arrival time with
an accuracy of 2 to 3 per cent. As this is better than the expected
accuracy of the peak overpressure measurements, shock arrival times and
the telemetered ambient pressure data were used for position determina-
tion with respect to the detonation. The azimuths of the canisters from
the shot are needed only for the purpose of applying a small wind cor-
rection to the computed slant ranges, and could be estimated with suffi-
cient accuracy from the radar track of the dropping aircraft.

Shot 4 was fired at such a great height of burst that it was not
expected that the triple point would reach the canister altitude within
the range of interesting overpressures. Consequently, no attempt was
made to extend the array to intercept the path of the triple point. For
Shot 9 a preshot estimate of the path was made on the basis of HE data
and the canister array was designed to intercept the expected path at
two levels. By extrapolating the time interval between the direct and
reflected shocks to zero it was expected that at least two points on the
path could be determined.

2.2 OPERATIONAL TECHNIQUES

The problem of the operation consisted of four phases:

1. The determination of the integrated horizontal drift of the
parachute borne canisters in the wind structure in order to determine
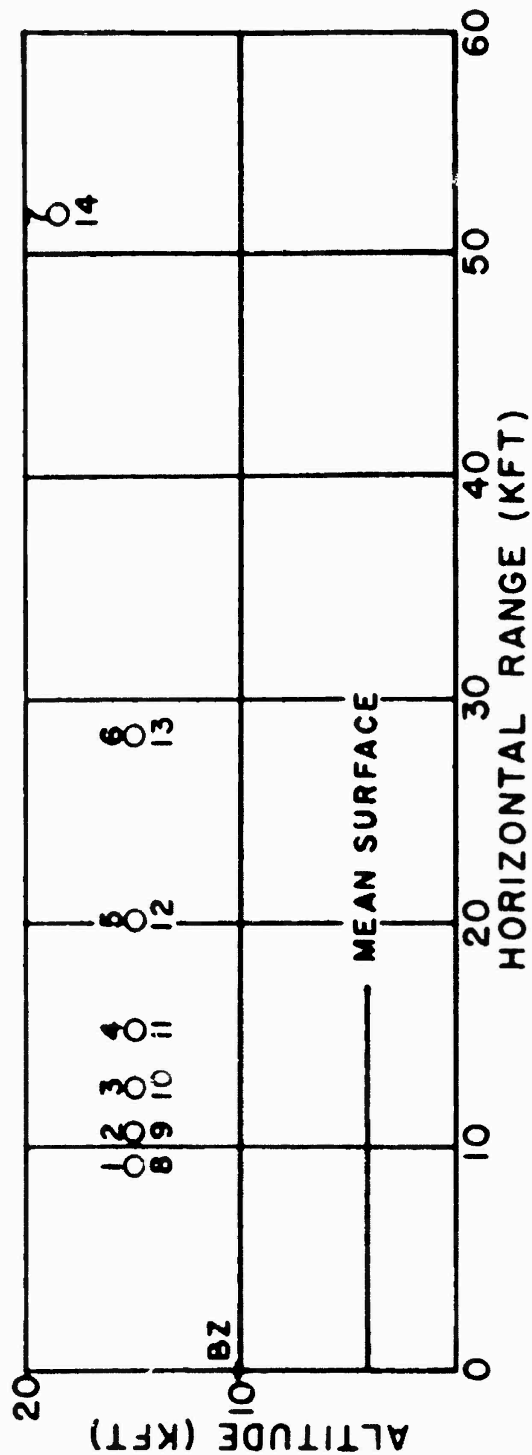corrected canister drop points for the aircraft;

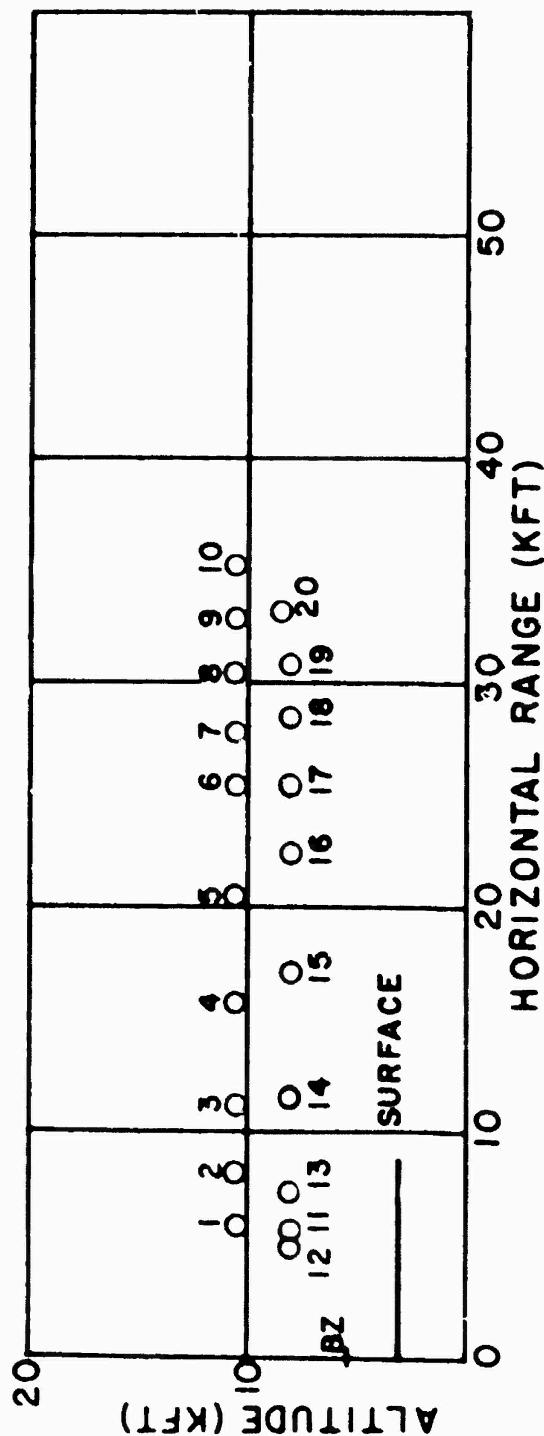Fig. 2.1 Planned Canister Array, Shot 4

Fig. 2.2 Planned Canister Array, Shot 9

13

2.   The guidance of two B-29 aircraft over the drop points both in reference to position and time;

3.   The deployment of parachute-borne canisters from the aircraft;

4.   The recording of telemetered blast pressure profiles from each canister.

2.2.1 Shot 4

The two aircraft operated in close formation at 20,000 ft MSL at a true ground speed of 292 ft/sec on the final or upwind leg of their pattern. Four practice runs were made between H-40 min and H-12 min. Flight patterns were tracked on an SCR-584 radar plotting board and guidance data with reference to time and position were transmitted to the aircraft commanders.

The initial drop point was determined to be at a point displaced 4000 ft west and 9000 ft south from ground zero. The selection of this point was based on two factors:

1. The possibility of prematurily triggering the fusing system of the weapon. Thus, it was required that no canisters be inside a cylindrical area in space having a radius of 9000 ft around ground zero.

2. The double drift data from the aircraft and the wind data from the weather station.

The 14 canisters were deployed with the aircraft flying upwind so that they would drift back to the desired positions at 15,000 ft altitude at predicted shock arrival time. The initial deployment was made at scheduled H-129 sec and final deployment was made at scheduled H+18 sec. The canisters were deployed at scheduled times although the aircraft arrived at the planned initial drop point 25 sec early. This fact plus the fact that the weapon detonated approximately 20 sec early resulted in the slant ranges being from 5000 to 10,000 ft greater than had been planned. The deployment times of canisters 6 and 7 were accidentally interchanged.

The recording of pressure and altimeter data from the canisters was accomplished as outlined in paragraph 2.2. Satisfactory records were obtained from all canisters although the range of overpressures covered was lower than intended because of the greater slant range.

2.2.2 Shot 9

The two B-29 aircraft operated in close formation at 17,500 ft MSL at a true ground speed of 298 ft/sec on the final or upwind leg of their pattern. Otherwise the operation was similar to Shot 4 with the following exceptions:

1. The initial drop point was determined to be at a point 6000 ft south and 1000 ft west of ground zero. The horizontal radius of the restricted area for canisters for Shot 9 was 5000 ft as compared to 9000

UNCLASSIFIED

ft for Shot 4.

2. The 20 canisters were deployed so that 10 were to be at 8100 ft MSL and 10 at 10,800 ft MSL at predicted shock arrival time. Initial canister deployment was made at H-161 sec, and final deployment at H-43 sec.

3. The two aircraft arrived at the initial drop point within ± 1 sec of the intended initial drop time so that the deviations of the actual canister positions shown in Fig. 3.2 from the intended positions shown in Fig. 2.2 are presumably due to errors in the allowance for wind drift or in intervalometer settings. In connection with the former it should be remarked that the wind correction was computed only for the initial drop and all other canisters were then dropped at preset time intervals after the first. This results in an over-correction for the later canisters which have a shorter time of fall. The very large deviation of canister No. 10 was due chiefly to delayed release because of malfunctioning of the bomb release mechanism.

2.3 INSTRUMENTATION

Each canister contained a pressure altimeter transducer, two differential pressure transducers (one having a scale ratio of approximately 2 with respect to the other) and a radio telemetry transmitter unit. The telemetry unit transmitted continuously overpressures and altitude data. The recording ground station was instrumented with a separate FM receiver for each parachute-borne canister and the differential pressure and altitude data received were recorded on Consolidated Engineering Company recording oscillographs.

To position the parachute-borne canisters at a uniform altitude, a dual-parachute system was necessary as the canisters were deployed at different times. As each canister was deployed from the aircraft a 6 ft flat ribbon parachute was immediately opened by the attached static line. Canister ballistic data and the particular array position determined the time of canister fall with the 6 ft parachute. At a predetermined time, different for each canister, an interval timer fired a squib which tripped a cutter mechanism which in turn detached the 6 ft ribbon parachute and released a 28 ft square semi-ribbon parachute. The rate of descent of the canisters with the 6 ft parachute is approximately 200 ft/sec as opposed to a fall rate of 30 ft/sec for the 28 ft parachute.

Reference is made to JANGLE Report WT-367, Project 1.3c, for a detailed description of the basic design of the telemetry system and canister instrumentation. The equipment was unchanged except the MOTS was eliminated due to reliability of shock arrival time for determining position of the canisters.

A SCR-584 radar station was used to guide the two B-29 aircraft to an initial drop point in reference to time and space.

CHAPTER 3

RESULTS

3.1 GENERAL

Canister altitudes at the time of arrival of the first shock have been determined from the telemetered ambient pressure records reduced to true altitude in accordance with the meteorological data obtained by the weather station at the Nevada Proving Grounds for the time of each shot. Slant ranges have been computed from the travel times and peak overpressure of the first shock by the method described in reports on previous tests. [2], [3] The canister positions attained are plotted in Figs. 3.1 and 3.2 for Shots 4 and 9 respectively.

3.2 OBSERVED DATA, SHOT 4

The overpressure vs. time curves as scaled from the original records and calibration curves are plotted in Fig. 3.3. In the case of canister No. 6 there was an initial pressure differential between the reference chamber and the ambient atmosphere due to the fact that this canister was still in rapid descent on the small drag chute at the time of shock arrival. A similar initial differential also existed in canister No. 7, due apparently to a restriction in the reference chamber vent line since this canister was in normal descent on the large chute. In both cases the sum of the initial differential and the peak shock overpressure was within the calibrated ranges of the differential pressure gages so that peak overpressures could still be measured.

Essentially ideal shock wave forms were obtained at all canister positions and all showed distinct reflected shocks. The observed arrival times and peak overpressures of both direct and reflected shocks are tabulated in Table 3.1. For the reflected shock the peak overpressure given is with reference to the pressure existing immediately prior to the arrival of this shock. The duration of the positive overpressure phase of the free-air shock is also given in Table 3.1 for all canisters at which the overpressure passed through zero before the arrival of the reflected shock. In canisters Nos. 1 through 5 and Nos. 8 and 13 the switch that arms the reference chamber sealing valve did not operate until after the arrival of the direct shock. Therefore, in these cases
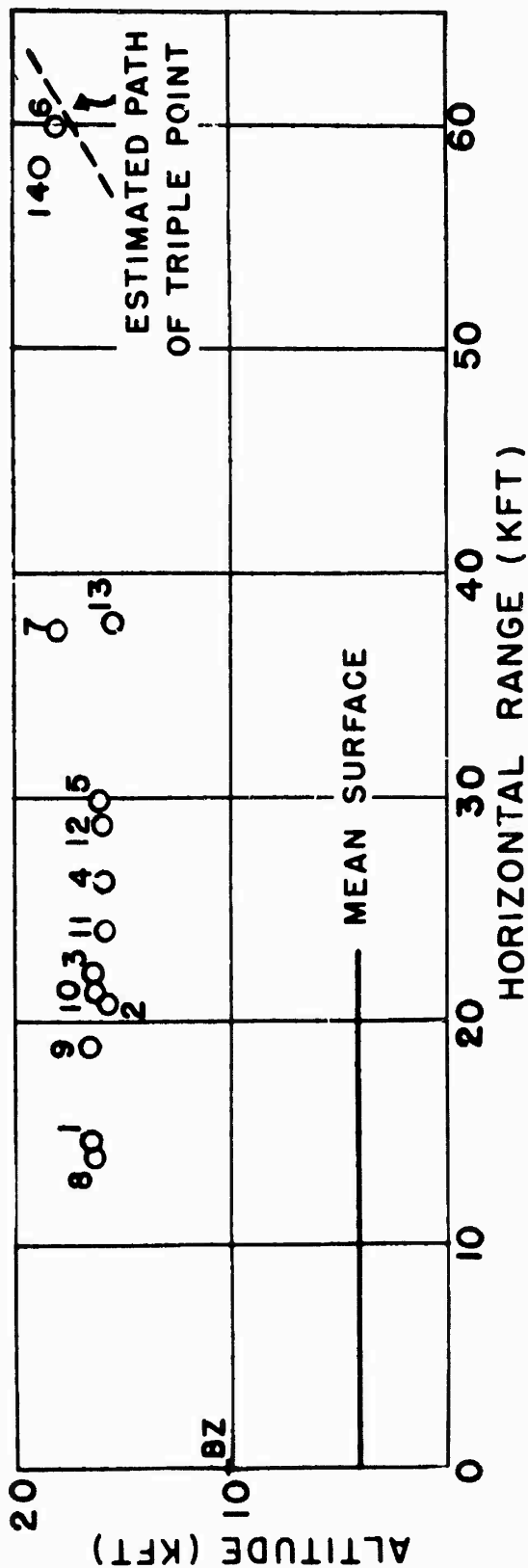
Fig. 3.1 Canister Positions, Shot 4
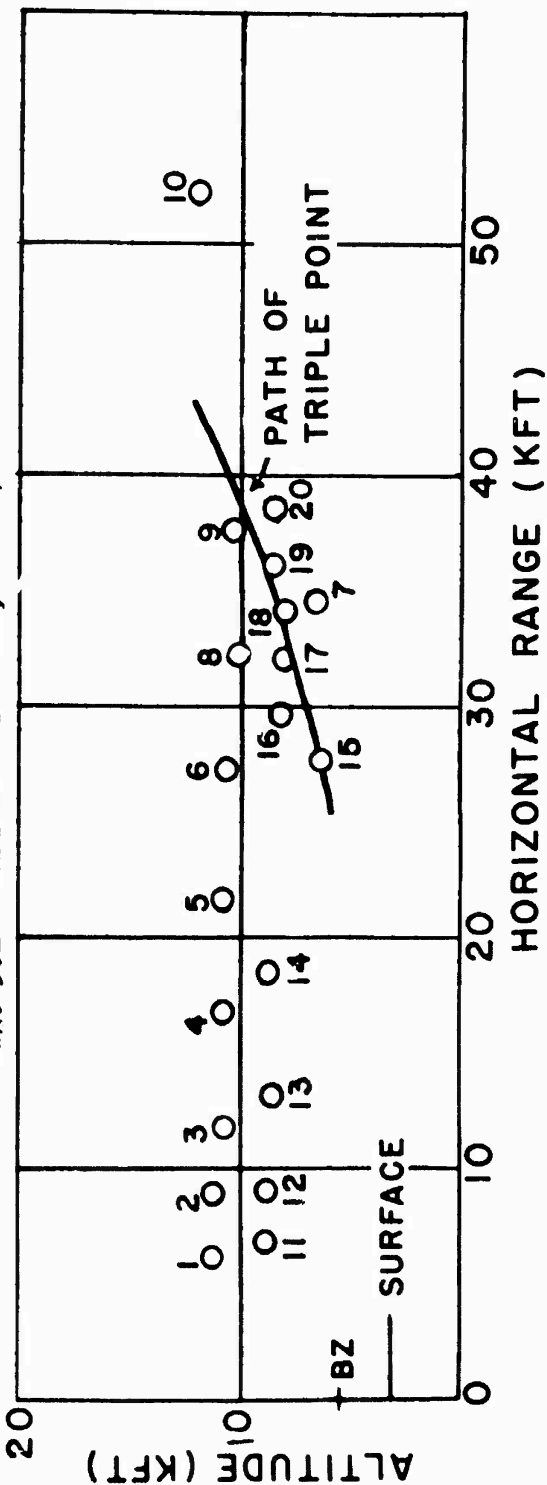
Fig. 3.2 Canister Positions, Shot 9

UNCLASSIFIED

Fig. 3.3 Overpressure vs. Time, Shot 4

18

CANISTER NO. 5

TIME IN SECONDS

CANISTER NO. 6

←SQUIB FIRE

TIME IN SECONDS

CANISTER NO. 7

TIME IN SECONDS

CANISTER NO. 8

TIME IN SECONDS

Fig. 3.3 Overpressure vs. Time, Shot 4 (cont)

19

Fig. 3.3 Overpressure vs. Time, Shot 4 (cont)

20

PRESSURE (PSI)

±.7 PSI GAUGE
+.5 +.4 +.3 +.2 +.1 0 -.1 -.2

CANISTER No. 13

±1 PSI GAUGE
+.5 +.4 +.3 +.2 +.1 0 -.1 -.2

35 36 37 38 39 40 41 42

TIME IN SECONDS

PRESSURE (PSI)

±.4 PSI GAUGE
+.5 +.4 +.3 +.2 +.1 0 -.1 -.2

CANISTER No. 14

±.7 PSI GAUGE
+.5 +.4 +.3 +.2 +.1 0 -.1 -.2

55 56 57 58 59 60 61 62

TIME IN SECONDS

Fig. 3.3 Overpressure vs. Time, Shot 4 (cont)

21

the reference chamber was still vented to the atmosphere through the delay line and the reference pressure was slowly increasing during the positive overpressure phase. The actual positive phase duration must then have been slightly greater than that indicated by the differential pressure gages. In canisters Nos. 9 through 12 the reference chamber was sealed and there should be no systematic error in the overpressure vs. time curves.

3.3 OBSERVED DATA, SHOT 9

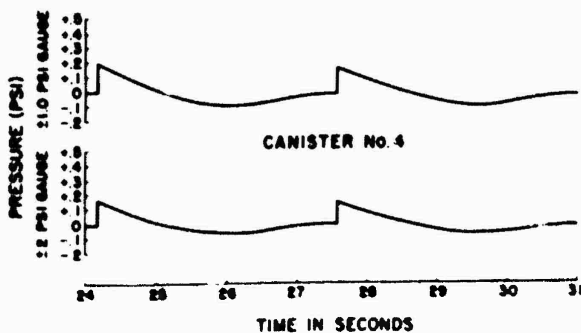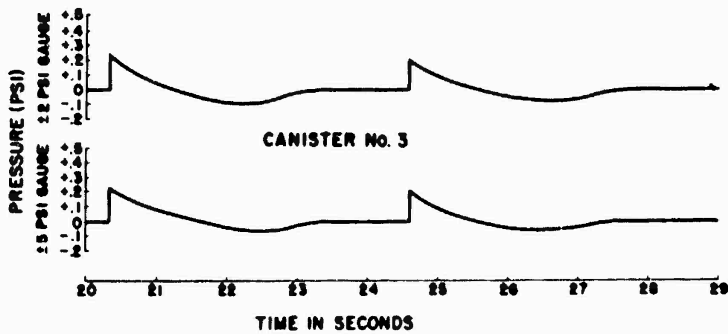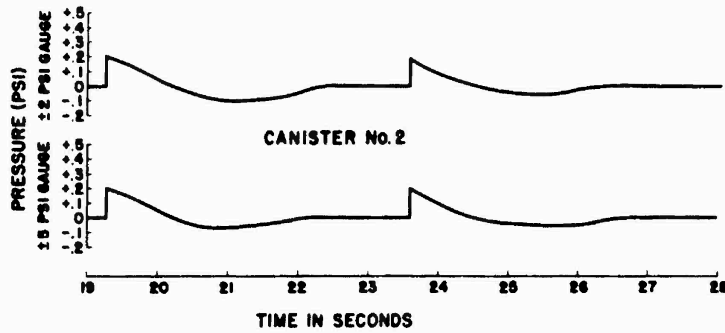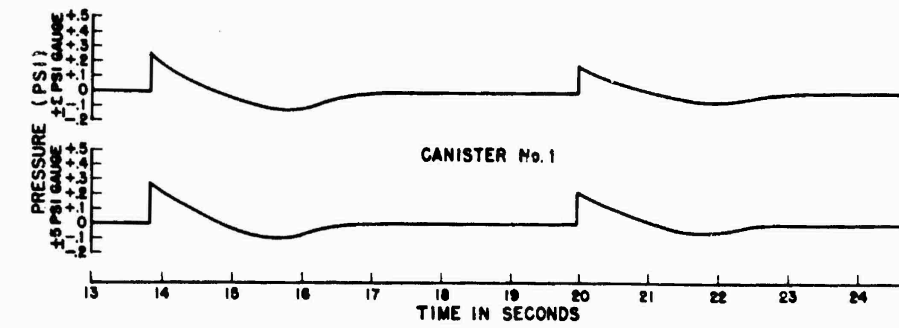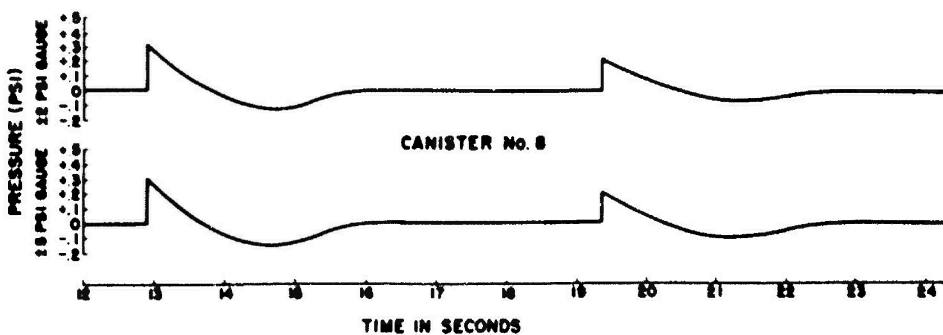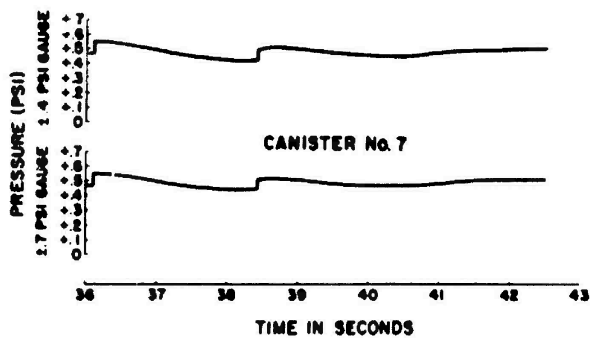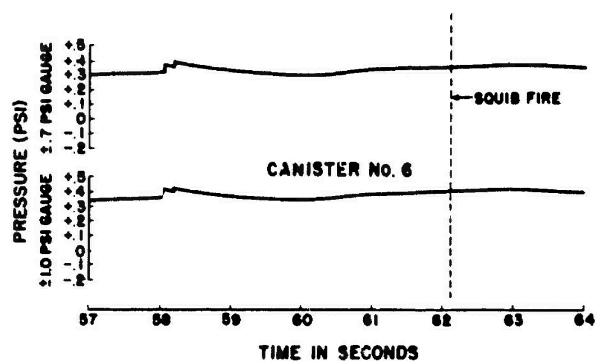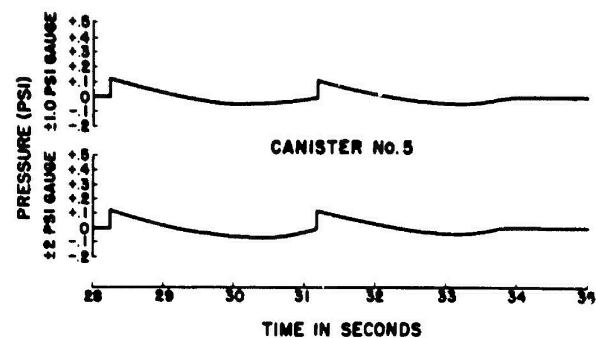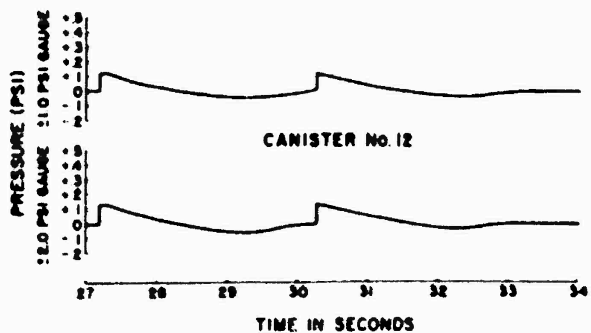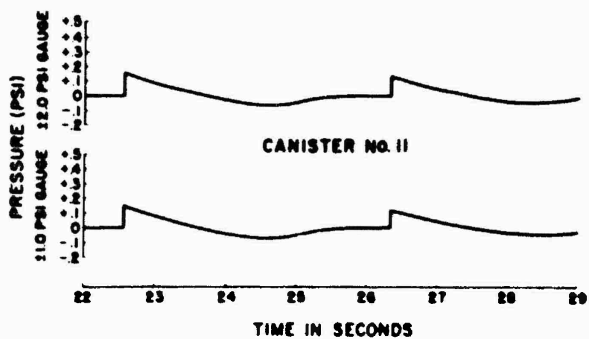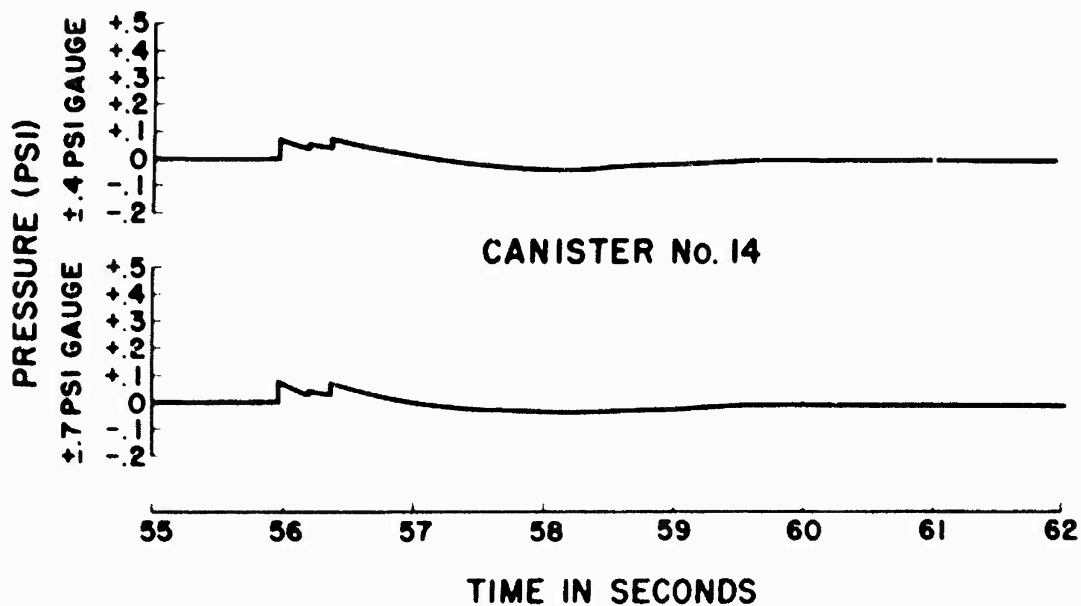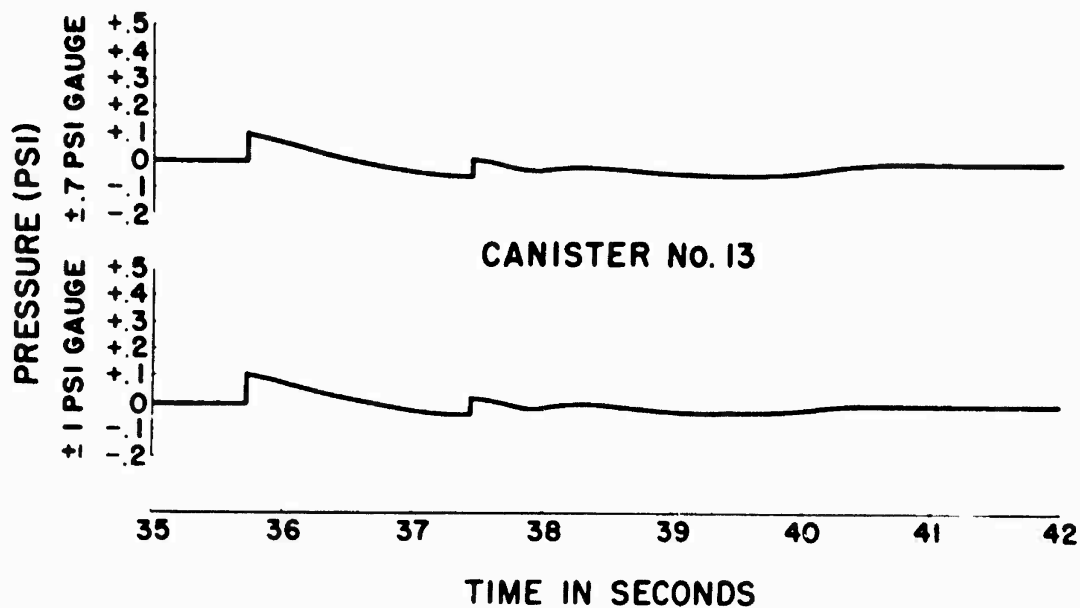The overpressure vs. time curves for Shot 9 are reproduced in Fig. 3.4. Canister No. 10 was in rapid descent on the small drag chute at shock arrival time, resulting in an initial pressure differential on the blast gages. However, the sum of the initial differential and the shock overpressure did not exceed the gage range so that a reliable overpressure measurement was obtained. Positional, time, and overpressure data for the canisters that fell in the free-air (regular reflection) region are given in Table 3.2 and for canisters in the Mach region in Table 3.3. All reference chambers were sealed at shock arrival time except for those in canisters Nos. 10, 11, 19 and 20. That in canister No. 11 sealed at 0.73 sec after the arrival of the first shock, while those in Nos. 10, 19 and 20 did not seal. The apparent positive phase durations for these canisters are therefore less than the actual durations.

For the canisters in the Mach region the method used to obtain slant range from the observed travel time and peak overpressure of the direct shock is not strictly applicable, since the superposition of the reflected and direct shocks to form the Mach stem results in an increase in peak overpressure and propagation velocity. This increase applies, however, only to that part of the propagation path that lies below the triple point, whereas the use of the average shock velocity corresponding to the full observed peak overpressure would amount to assuming that the increment in velocity applied to the whole path. Actually it would make only a small difference in the present case, since the peak overpressures at all the canisters in the Mach region were low and the corresponding average shock velocities are only a few per cent greater than sound velocity on any assumption. As a rough correction the average shock velocity corresponding to 65 per cent of the observed peak overpressure has been used in computing the slant ranges given in Table 3.3.

In addition to the main direct and ground reflected shocks the records from all canisters show at least one and usually two very much smaller shocks. In contrast to similar weak secondary shocks that have been observed occasionally on previous tests, these are quite clearly correlatable across the entire canister array. It will be shown later that the arrival times of these shocks are consistent with the assumption that they originated from a weak second pulse emitted about 1 sec after the main explosion. The first of these shocks (arrival time T_3) is the wave along the direct path and the second (arrival time T_4) is the ground reflected wave. To facilitate the identification of the latter, the length of the acoustic path (R_i) from shot to ground to canister is given in Table 3.4 together with the arrival times and approximate peak overpressures.

22

TABLE 3.1 - Shot 4, Observed Data

Canister No.	z	T_1	R	ΔP_1 Hi.Ra.	Lo.Ra.	Mean	T_+	T_2	ΔP_2 Hi.Ra.	Lo.Ra.	Mean
1	16,480	13.83	16,030	0.28	0.26	0.270	0.85+	19.96	0.20	0.17	0.185
2	15,700	19.28	21,540	0.20	0.20	0.20	0.92+	23.61	0.20	0.18	0.19
3	16,400	20.33	23,050	0.23	0.24	0.235	0.89+	24.60	0.21	0.20	0.205
4	15,850	24.18	26,840	0.17	0.20	0.185	0.88+	27.59	0.15	0.18	0.165
5	16,050	28.25	30,510	0.12	0.12	0.120	0.99+	31.19	0.12	0.12	0.12
6	17,950	58.06	60,380	0.06	0.05	0.055		58.20	0.02	0.03	0.025
7	18,000	36.11	38,170	0.08	0.08	0.08		38.42	0.07	0.07	0.07
8	16,350	12.90	15,170	0.30	0.31	0.305	0.90+	19.35	0.20	0.21	0.205
9	16,600	17.56	19,910	0.24	0.23	0.235	1.03	22.45	0.17	0.17	0.17
10	16,300	20.07	22,240	0.17	0.18	0.175	1.00	24.40	0.15	0.15	0.15
11	15,900	22.56	24,680	0.14	0.16	0.15	1.23	26.33	0.12	0.14	0.13
12	15,950	27.19	29,370	0.13	0.12	0.125	1.06	30.26	0.12	0.11	0.115
13	15,450	35.72	38,220	0.11	0.10	0.105	0.88+	37.45	0.06	0.06	0.06
14	18,790	55.96	58,590	0.08	0.07	0.075		56.37	0.04	0.03	0.035

z = Canister altitude (ft above sea level)
T_1 = Arrival time of direct shock after shot time (sec)
R = Slant range (ft) computed from T_1 and observed peak overpressure
ΔP_1 = Peak overpressure in direct shock (psi)
T_+ = Duration of positive overpressure in direct shock (sec)
ΔP_2 = Peak overpressure in reflected shock (psi) measured from pressure existing immediately prior to reflected shock arrival
T_2 = Arrival time of reflected shock after shot time (sec)

23

TABLE 3.2 — Shot 9, Observed Data, Canisters in Free-Air Region

Notation: As in Table 3.1

Canister No.	z	T_1	R	ΔP_1 Hi.Ra.	Lo.Ra.	Mean	T_+	T_2	ΔP_2 Hi.Ra.	Lo.Ra.	Mean
1	11,150	6.04	8,470	1.05	0.99	1.02	1.06	9.37	0.70	0.71	0.705
2	11,125	8.00	10,650	0.74	0.75	0.745	1.13	10.88	0.61	0.67	0.64
3	10,700	10.32	13,030	0.50	0.52	0.51	1.21	12.72	0.45	0.42	0.435
4	10,700	14.53	17,650	0.39	0.33	0.36	1.27	16.20	0.21	0.18	0.195
5	10,875	19.09	22,430	0.25	0.25	0.25		20.17	0.15	0.14	0.145
6	10,650	24.01	27,920	0.20	0.19	0.195		24.61	0.09	0.08	0.085
8	10,150	28.04	32,690	0.21	0.20	0.205		28.38	0.09	0.09	0.09
9	10,250	33.23	38,020	0.14	0.14	0.14		33.33	0.07	0.07	0.07
11	8,825	5.34	7,720	1.30	1.27	1.285	0.88	8.12	0.88	0.93	0.905
12	8,750	7.13	9,700	0.90	0.93	0.915	1.07	9.39	0.55	0.64	0.595
13	8,450	10.60	13,570	0.60	0.60	0.60	1.18	12.12	0.35	0.33	0.34
14	8,600	15.51	18,810	0.33	0.39	0.36		16.37	0.17	0.18	0.175
16	8,100	25.25	29,920	0.20	0.20	0.20		25.43	0.08	0.08	0.08
17	8,050	27.73	32,190	0.20	0.18	0.19		27.80	0.08	0.08	0.08

TABLE 3.3 Shot 9, Observed Data, Canisters in Mach Region

Canister No.	z	T_m	R	ΔP_m Hi.Ra.	ΔP_m Lo.Ra.	ΔP_m Mean	T+
7	6,550	29.98	34,570	0.26	0.25	0.255	1.61
10	11,925	47.39	52,560	0.13	0.09	0.11	
15	6,325	23.65	27,770	0.37	0.37	0.37	1.52
18	7,875	29.76	34,250	0.24	0.23	0.235	1.75
19	8,400	31.83	36,410	0.22	0.22	0.22	1.67+
20	8,350	33.93	38,750	0.20	0.21	0.205	1.57+

Notation:

T_m = Arrival time of Mach shock after shot time (sec)

ΔP_m = Peak overpressure in Mach shock (psi)

Other symbols as in Table 3.1
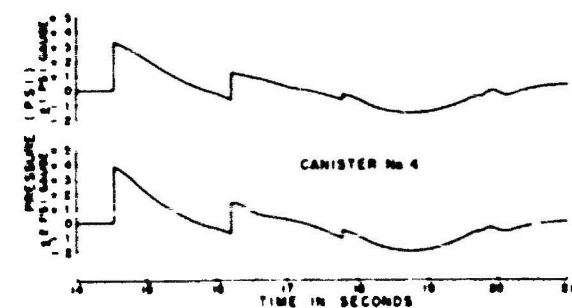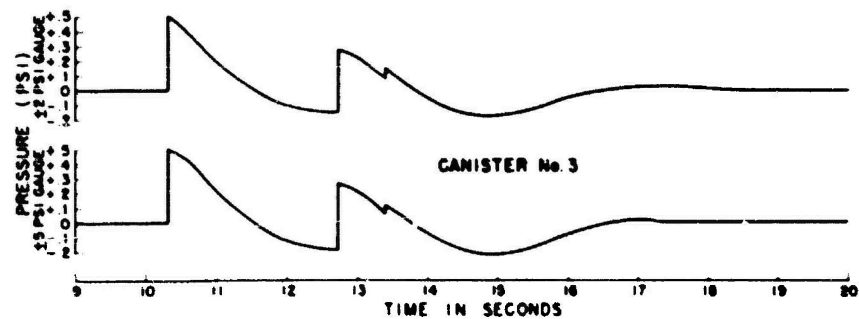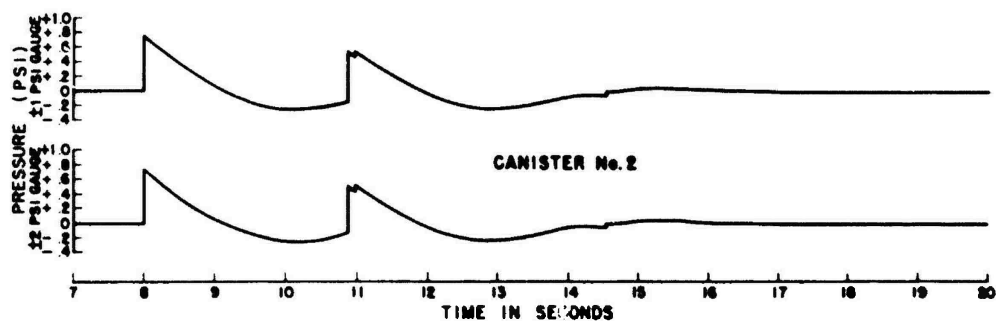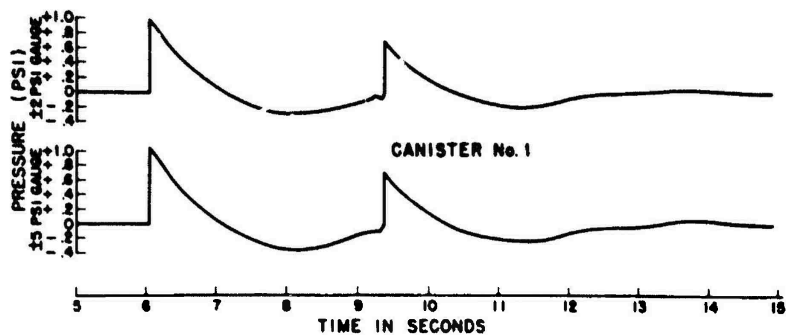
UNCLASSIFIED

CANISTER No.1
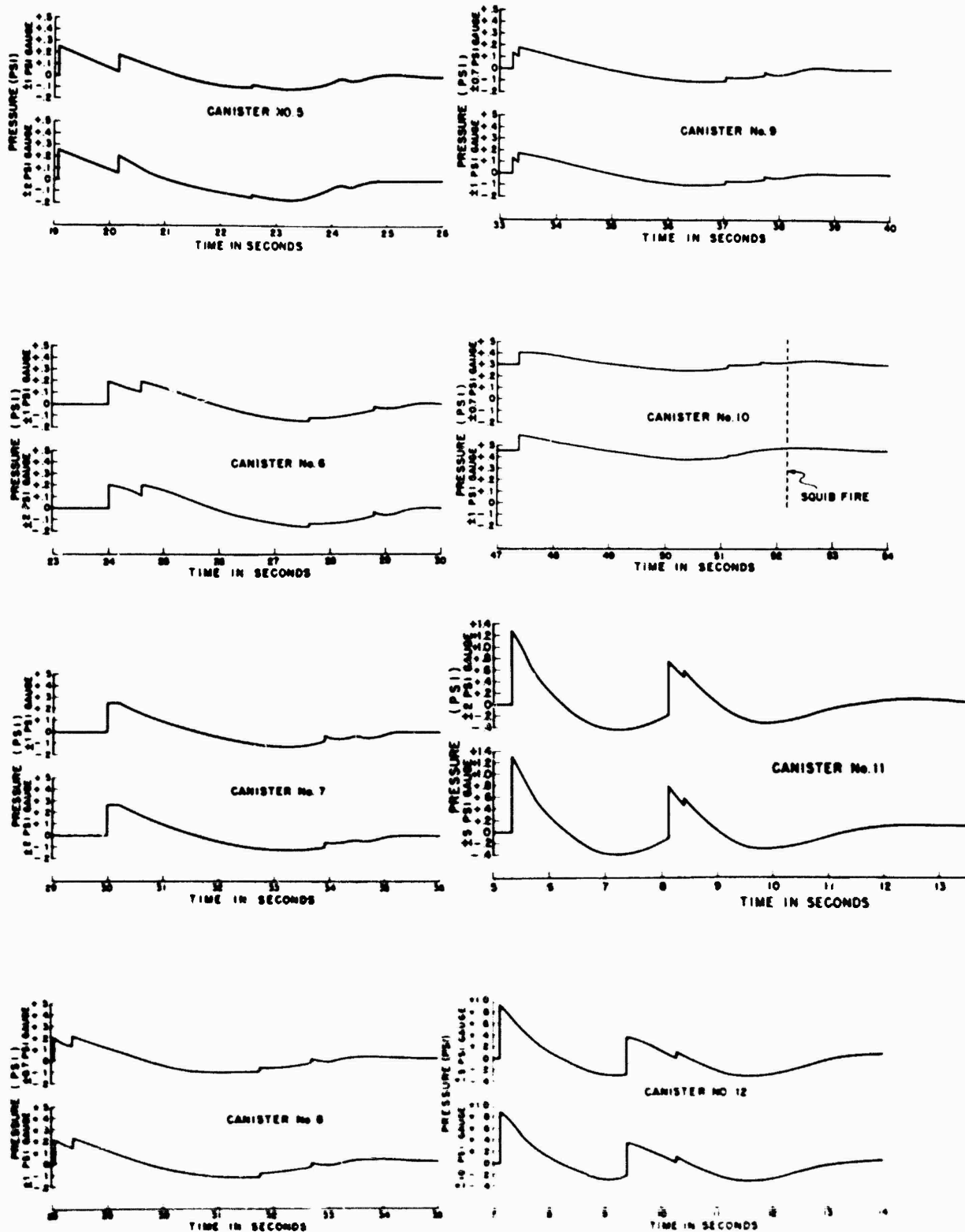
TIME IN SECONDS

CANISTER No.2

TIME IN SECONDS

CANISTER No.3

TIME IN SECONDS

CANISTER No 4

TIME IN SECONDS

Fig. 3.4 Overpressure vs. Time, Shot 9

26

Fig. 3.4 Overpressure vs. Time, Shot 9 (cont)

27

Fig. 3.4 Overpressure . . . Time, Shot 9 (cont)

28
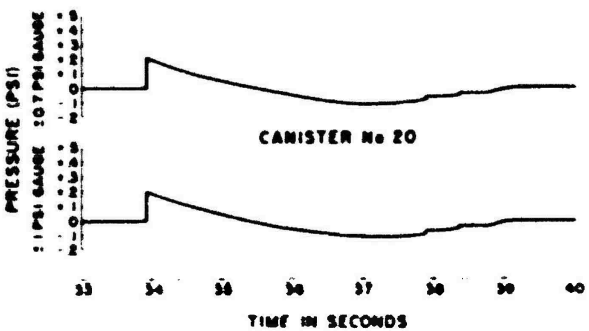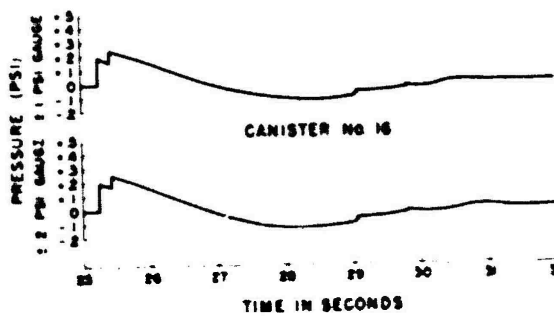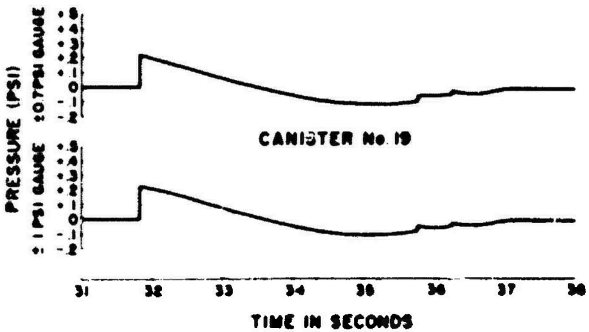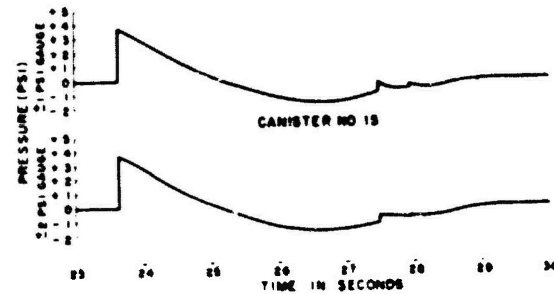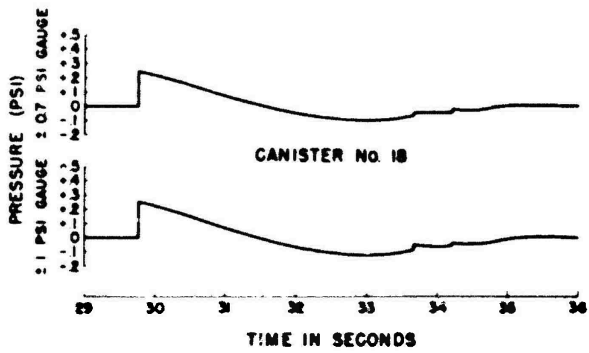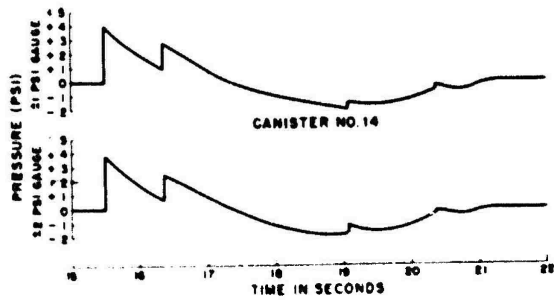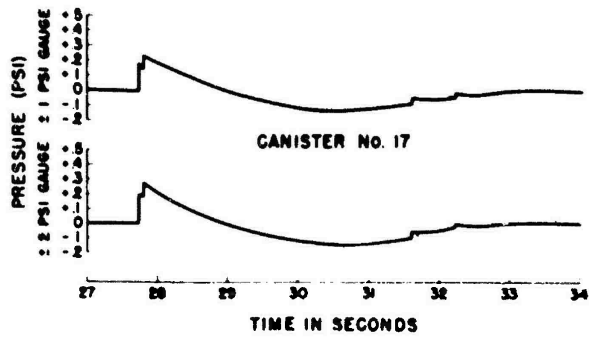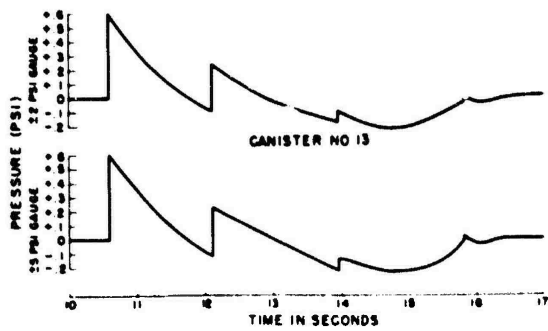
TABLE 3.4 - Shot 9, Observed Data, Secondary Shock

Notation:

T_3 = Arrival time of secondary shock by direct path (sec)

ΔP_3 = Peak overpressure in direct secondary shock measured from pressure existing immediately prior to shock arrival (psi)

T_4 = Arrival time of reflected secondary (sec)

R_1 = Slant Range from image of source (ft)

ΔP_4 = Peak overpressure in reflected secondary shock

Canister No.	T_3	ΔP_3	T_4	R_1	ΔP_4
1	9.23 (?)			12,250	
2	10.97	0.07	14.55	13,830	0.04
3	13.39	0.06		15,610	
4	17.79	0.04		19,630	
5	22.57	0.02		24,050	
6	27.61	0.02	28.79	29,200	0.02
7	33.91	0.04	34.34	35,050	
8	31.76	0.03	32.69	33,720	0.03
9	37.03	0.02	37.75	38,920	0.02
10	51.12	0.02	51.53 (?)	53,370	
11	8.41	0.12	11.76	10,730	
12	10.28	0.10		12,210	
13	13.96	0.08	15.82	15,370	0.02
14	19.07	0.05	20.37	20,180	0.02
15	27.48	0.06	27.94	28,320	0.02
16	29.05	0.04	29.79	30,720	0.02
17	31.60	0.04	32.22	32,940	0.02
18	33.65	0.04	34.20	34,920	0.02
19	35.77	0.03	36.27	37,110	0.02
20	37.88	0.02	38.33	39,400	0.02

CHAPTER 4

DISCUSSION

4.1 GENERAL

Prior to the present tests, shock overpressure measurement at high altitudes by the same system had been obtained at the surface shot of JANGLE, Shots 5 and 8 of SNAPPER, and Shots Mike and King of IVY. The JANGLE and IVY Mike shots were surface bursts, the SNAPPER shots were fired on 300 ft towers, and the IVY King shot was burst at an a..itude of 1500 ft, but because of the very large yield of this shot, this too was effectively a low height of burst. Except for three canisters at King shot, all the airborne pressure measurements were obtained in the Mach region at large distances from the triple point. Although it is considered that the results of these earlier tests validate the Fuchs[4] scaling law as a practical method of computing the effects of the difference in ambient atmospheric conditions between shot and gage, the reduction of the observed peak overpressures to true free-air values necessarily involved a rather arbitrary choice of the ground reflection factor to be applied to the actual yield. We therefore use the present free-air data to derive a new free-air peak overpressure curve normalized to 1 KT in a homogeneous sea-level atmosphere, without reference to the earlier test results. This curve will then be used to determine the apparent reflection factors for the previous shots.

4.2 REDUCTION TO 1 KT IN A HOMOGENEOUS SEA-LEVEL ATMOSPHERE

The Sachs[5] scaling law for altitude of burst and the Fuchs scaling law for the effect of the difference in altitude between burst and gage may be expressed in the form

$$\Delta P = k^3 \mu \, f(k \lambda R/S) \tag{4.1}$$

where

ΔP = peak overpressure

constant range

UNCLASSIFIED

$$k = \left[P_0(h)/P_0(o)\right]^{1/3}$$

$$\lambda = \exp \int_h^z \left[\left\{T(h)/T(z)\right\}^{3/4}\left\{P_0(h)/P_0(z)\right\}^{1/2} -1\right] dz/(z-h)$$

$$\mu = \lambda\left\{T(h)/T(z)\right\}^{1/4}\left\{P_0(z)/P_0(h)\right\}^{1/2}$$

P_0 = ambient atmospheric pressure

T = ambient atmospheric temperature (absolute)

z = altitude of gage at which ΔP is measured

h = altitude of burst

W = bomb yield (KT)

$S = W^{1/3}$

The slant range scaled to 1 KT in a homogeneous atmosphere at sea-level ambient pressure (taken as 14.70 psi) is then

$$r = k\lambda R/S \tag{4.2}$$

and the scaled peak overpressure is

$$f(r) = \Delta P/k^3\mu \tag{4.3}$$

The function $f(r)$ will be referred to as the normalized free-air peak overpressure function.

According to the asymptotic blast theory on which the Fuchs scaling law is based, the duration of the positive overpressure phase is not affected by the variation of atmospheric properties along the propagation path. Normalization of the positive phase duration to 1 KT at sea-level therefore involves only the Sachs time scale factor and is given by

$$\mathcal{T} = T_+ kc(h)/Sc(o) \tag{4.4}$$

where c is the velocity of sound. The sea-level value, $c(o)$, is taken to be 1116 ft/sec corresponding to a temperature of 15°C.

The Fuchs scale factors λ and μ have been computed by numerical integration of the meteorological data for the time of each shot. For Shot 4 the altitude of burst was 10,213 ft above sea level (6022 ft above ground zero) and for Shot 9, 5502 ft above sea level (2423 ft above ground zero). The yields used in scaling to 1 KT are 10.5 KT for Shot 4 and 26.5 KT for Shot 9.*

---

* After all data reduction and figure drafting for the present report had been completed the figures 11.0 KT and 26 KT respectively were adopted for use in the preparation of final project reports (AFSWP UPSHOT-KNOTHOLE Summary data Chart, 22 Sep 1953). Since the difference is well within the uncertainty of the data and would be entirely negligible for practical purposes, no change has been made.

The various scale factors and the scaled ranges, peak overpressures, and positive phase durations for the free-air shock are tabulated for Shot 4 in Table 4.1 and for Shot 9 in Table 4.2. Scaled peak overpressure is plotted against scaled slant range in Figs. 4.1 and 4.2. The curves drawn in these figures do not represent "predicted" values, but are simply "eye fits" to the plotted points, giving greatest weight to those points that appear to define a reasonably smooth curve and ignoring the more erratic points such as canisters Nos. 3, 4, and 14 of Shot 4 and canister No. 8 of Shot 9.

The scaled ranges and peak overpressures in the Mach stem of Shot 9 are tabulated in Table 4.3 and plotted in Fig. 4.3. Since the scaled peak overpressure in the Mach stem in the region just below the triple point is probably not a function of the scaled slant range only, the significance of drawing a single curve through these points, as shown in Fig. 4.3, is somewhat questionable. The interpretation of these measurements in the Mach region will be discussed in more detail in section 4.6.

In Fig. 4.4 the smoothed curves of Figs. 4.1 and 4.2 are reproduced together with the lower portion of the Naval Ordnance Laboratory TUM-BLER composite curve.[6] The latter curve, obtained from photographic shock velocity measurements, is considered to be the most precise determination of the normalized free-air peak overpressure function for nuclear detonations now available for scaled overpressures greater than about 7 psi. It is unfortunate that restrictions on allowed canister positions did not permit the present measurements to extend up to the lower limit of the NOL curve. However, inspection of Fig. 4.4 will indicate that if we require a smooth interpolating curve that will join the NOL curve without abrupt change in slope and will parallel the slopes of the Shot 4 and Shot 9 curves, there is little latitude for deviation from the curve indicated by the dashed line in the figure. In drawing this curve slightly more weight has been given to the data from Shot 9 than to that from Shot 4 because of the greater internal consistency of the former.

For the convenience of those who may wish to use the present data in future applications, a tabulation of the function $f(r)$, defined by the interpolated curve in Fig. 4.4 for values less than 7 psi and by the NOL curve for higher overpressures, is presented in Table A.4. The table has been prepared by smoothed numerical interpolation between values read at convenient intervals from the plotted curves. Although the tabulation is carried to three figures in the interest of reproducibility of computations, the basic data do not, of course, define this function with anything approaching this degree of accuracy.

4.3. COMPARISON WITH PREVIOUS TEST RESULTS

Using the present normalized free-air peak overpressure curve, we may define an apparent yield scale factor, S_a, for each peak overpressure measurement obtained in the previous tests by reading the scaled range, r, corresponding to the observed scaled overpressure, $\Delta P/k^3\mu$, and computing

$$S_a = k\lambda R/r \qquad (4.5)$$

32

TABLE 4.1 Shot 4, Free-Air Data Reduced to 1 KT in a Homogeneous
Sea-Level Atmosphere

Canister No.	Fuchs Scale Factors		Scaled Range (ft)	Scaled Peak Overpres. (psi)	Scaled Positive Phase Dur. (sec)
	λ	μ	$r = k\lambda R/S$	$f(r) = \Delta P/k^3\mu$	$T = T_+kc(h)/c(o)S$
1	1.189	1.061	7,640	0.375	0.33+
2	1.163	1.055	10,050	0.279	0.36+
3	1.186	1.061	10,960	0.326	0.35+
4	1.168	1.057	12,570	0.258	0.34+
5	1.175	1.058	14,380	0.167	0.39+
6	1.238	1.075	29,970	0.075	
7	1.240	1.075	18,980	0.110	
8	1.184	1.060	7,200	0.424	0.35+
9	1.192	1.062	9,520	0.326	0.40
10	1.183	1.060	10,550	0.243	0.39
11	1.170	1.057	11,580	0.209	0.48
12	1.171	1.057	13,790	0.174	0.41
13	1.155	1.052	17,700	0.147	0.34+
14	1.268	1.083	29,790	0.102	

$h = 10,213$ ft $P_o(h) = 9.98$ psi
$k^3 = 0.679$ $k = 0.879$
$W = 10.5$ KT $S = 2.19$

33

TABLE 4.2 Shot 9, Free-Air Data Reduced to 1 KT in a Homogeneous
Sea-Level Atmosphere

Canister No.	Fuchs Scale Factors		Scaled Range (ft)	Scaled Peak Overpres. (psi)	Scaled Positive Phase Dur. (sec)
	λ	μ	$r = k\lambda R/S$	$f(r) = \Delta P/k^3\mu$	$\tau = T_+ kc(h)/c(o)S$
1	1.178	1.062	3,150	1.15	0.33
2	1.177	1.062	3,960	0.84	0.35
3	1.163	1.057	4,790	0.58	0.38
4	1.163	1.057	6,480	0.410	0.40
5	1.169	1.058	8,280	0.284	
6	1.161	1.056	10,240	0.222	
8	1.143	1.051	11,800	0.235	
9	1.148	1.052	13,780	0.160	
11	1.101	1.036	2,680	1.49	0.27+
12	1.099	1.035	3,370	1.06	0.33
13	1.089	1.031	4,670	0.70	0.37
14	1.094	1.033	6,500	0.419	
16	1.078	1.027	10,190	0.234	
17	1.077	1.027	10,950	0.222	

$h = 5500$ ft $P_0(h) = 12.23$ psi
$k^3 = 0.832$ $k = 0.941$
$W = 26.5$ KT $S = 2.98$

UNCLASSIFIED.

SECRET - RESTRICTED DATA

TABLE 4.3 Shot 9, Mach Data Reduced to 1 KT in a Homogeneous
Sea-Level Atmosphere

Canister No.	Fuchs Scale Factors		Scaled Range (ft) $r = k\lambda R/S$	Scaled Peak Overpres. (psi) $f(r) = \Delta P/k^3\mu$	Scaled Positive Phase Dur. (sec) $T = T_+ kc(h)/c(o)S$
	λ	μ			
7	1.032	1.011	11,270	0.303	0.50
10	1.204	1.072	19,980	0.123	
15	1.025	1.009	8,990	0.441	0.47
18	1.071	1.025	11,580	0.275	0.55
19	1.088	1.031	12,510	0.256	0.52+
20	1.087	1.030	13,300	0.239	0.49+

Since the individual values of S_a for a given shot showed no systematic
trend that could be distinguished above the random scatter of the data,
only the mean values, S_a, for each shot are listed in Table 4.4. For
King Shot only the measurements in the Mach region have been used. For
our present purpose the apparent blast yield, W_a, is defined as the
cube of the mean apparent scale factor. The apparent yield reflection
factor is then the ratio of W_a to the actual yield, W. The values of
W given in Table 4.4 are the most recent estimates known to the writers.
but their accuracy cannot be stated with assurance.

It is commonly assumed that for a surface burst the reflection
factor in the sense used here would have the value 2 for an ideal re-
flecting surface and would be slightly less than 2 for real surfaces.
In the case of a burst at a finite height above the surface there is no
a priori reason for expecting the apparent reflection factor for points
In the Mach stem to be equal to or less than 2, but it is at least
plausible to suppose that in the ideal case the peak overpressure at
points far outside the path of the triple point would approach the same
value as that due to a surface burst. It is therefore somewhat surpris-
ing to find that with reference to the present free-air peak overpres-
sure curve the mean apparent reflection factors for all the earlier
shots turn out to be greater than the "ideal" value 2. In the case of
Mike Shot there are reasons for believing that the high apparent re-
flection factor is due to inaccuracy in the Fuchs altitude correction
for very large yield weapons, but this does not explain the results for
the small yield shots. Although there is a considerable difference be-
tween individual shots, it is believed that the general average is
reliable enough to indicate that there is some real effect, occurring
with low scaled heights of burst (say less than 200 ft for 1 KT), that
gives an increase in the apparent blast yield that is slightly greater
than one would expect from elementary considerations.

35

TABLE 4.4 - Apparent Reflection Factor for Low Heights of Burst

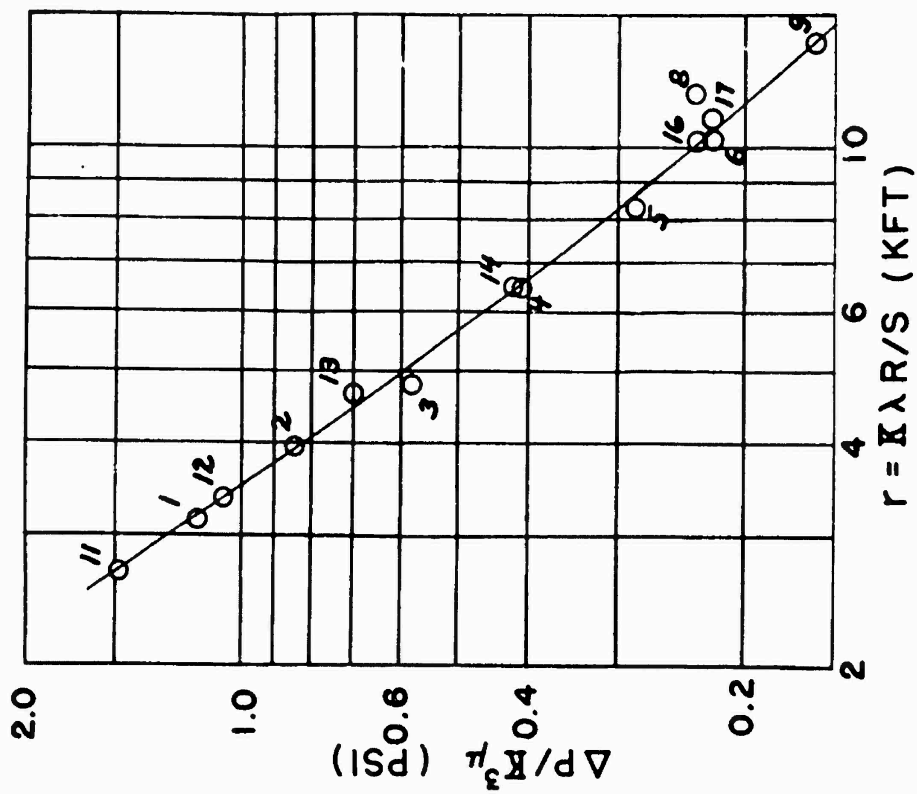| Shot	No. Data Points	Scaled Height of Burst (ft)	Mean Apparent Yield Scale Factor S_a	Apparent Blast Yield (KT) $W_a = S_a^3$	Actual Yield W	Apparent Yield Reflection Factor W_a/W
JANGLE Surf	7	0	1.46	3.11	1.20	2.59
SNAPPER No. 5	11	103	3.11	30.1	11.7	2.57
SNAPPER No. 8	13	97	3.16	31.6	14.0	2.26
IVY Mike	10	0	28.5	23.2×10^3	10.4×10^3	2.23
IVY King	5	183	11.4	1.48×10^3	0.55×10^3	2.69

Fig. 4.2 Shot 9, Free-Air Peak Overpressure vs.
Slant Range, Reduced to 1 KT in a Homogen-
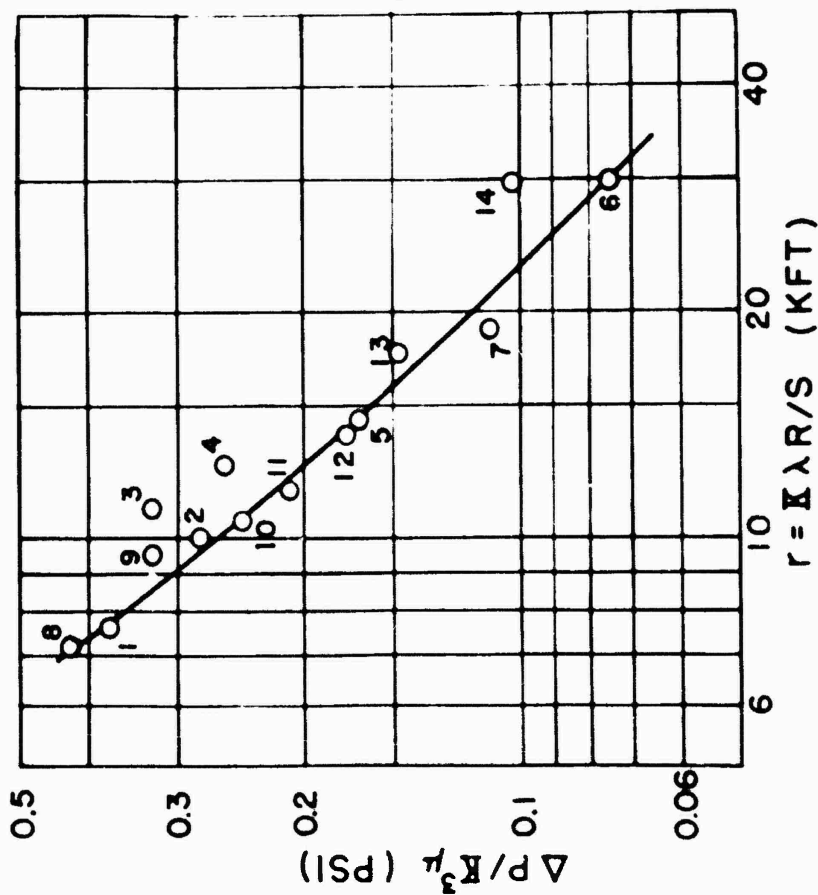eous Sea-Level Atmosphere

Fig. 4.1 Shot 4, Free-Air Peak Overpressure vs.
Slant Range, Reduced to 1 KT in a Homogen-
eous Sea-Level Atmosphere

37

A similar phenomenon has been noted by the authors of the final report on Projects 1.3 and 1.5 of TUMBLER in comparing the TUMBLER free-air peak overpressure data with that obtained by the same shock velocity method from Shot Easy of GREENHOUSE.[7] The GREENHOUSE Easy
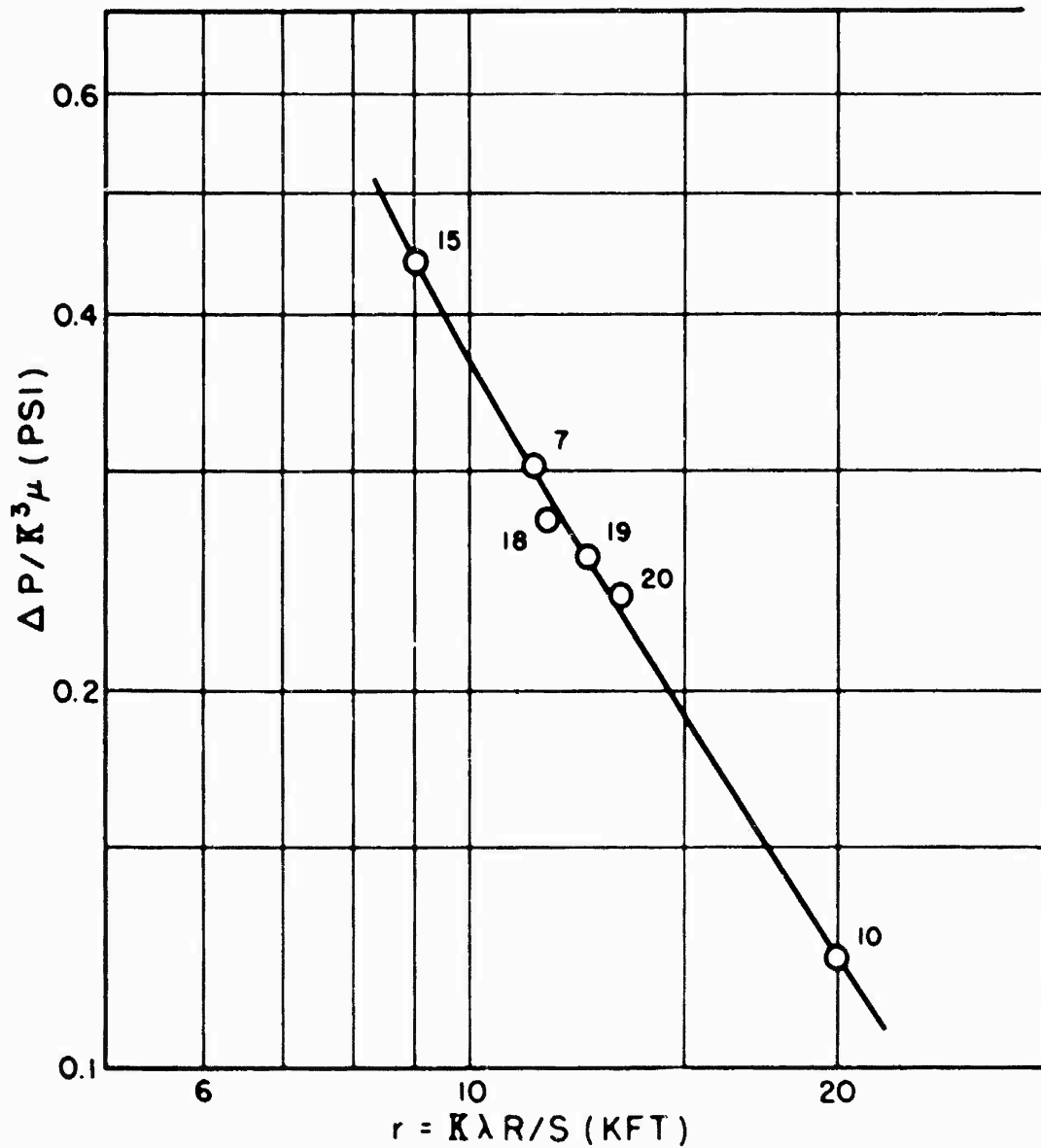

Fig. 4.3 Shot 9, Peak Overpressure vs Slant Range in the Mach Region, Reduced to 1 KT in a Homogeneous Sea-Level Atmosphere
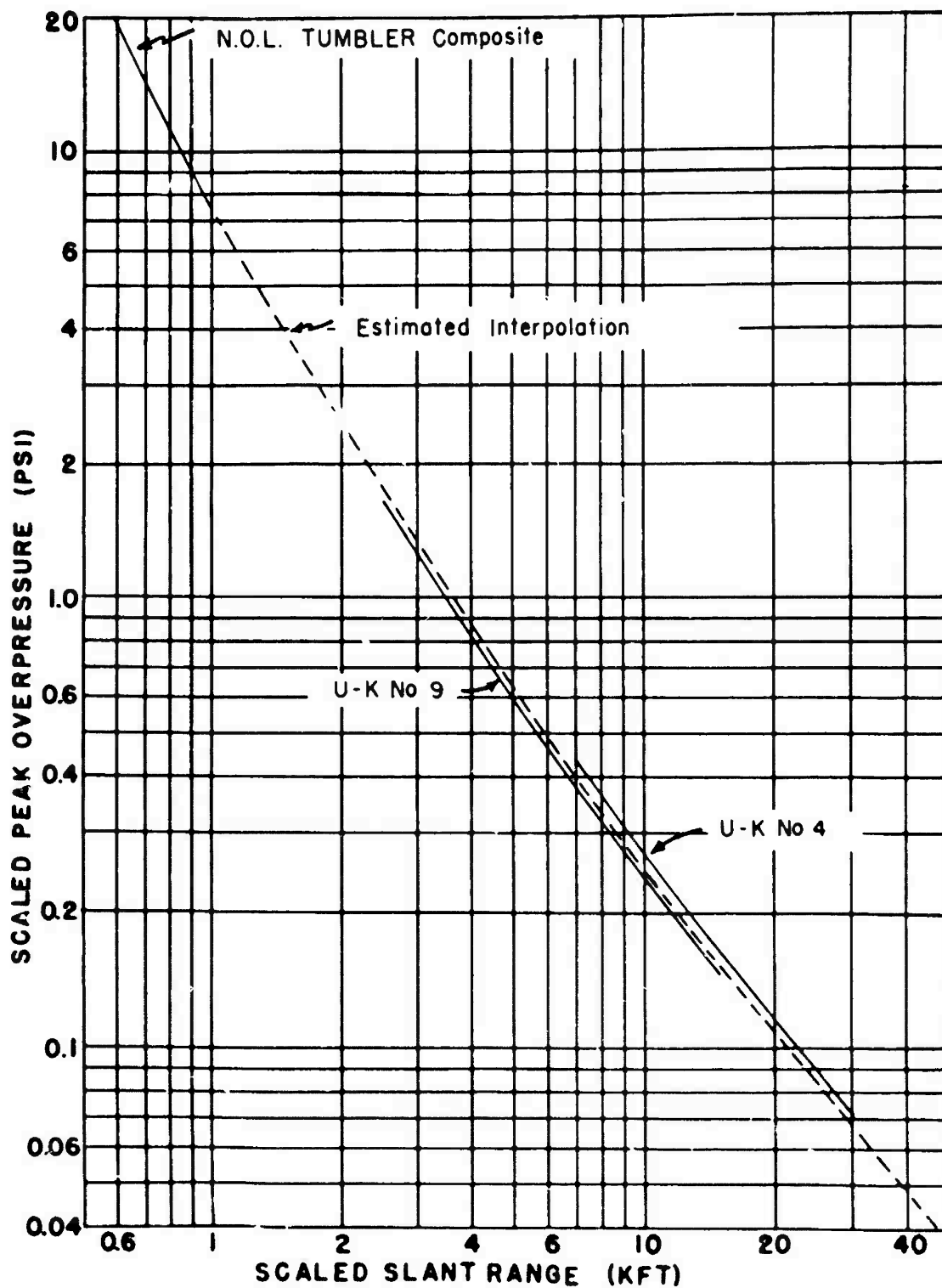
SECRET   RESTRICTED DATA

Fig. 4.4 Normalized Composite Free-Air Peak Overpressure vs.
Slant Range

39

free-air peak overpressures are definitely higher in the 140 to 35 psi range than those which would be scaled from the TUMBLER curve. Since this increment in apparent blast yield for low scaled heights of burst is shown by the free-air shock, it must be caused by something that occurs at a very early stage in the formation of the primary shock, since otherwise the effect could not overtake the free-air shock front in time to begin affecting the peak overpressure at about the 140 psi level. If the high apparent reflection factors in the far Mach region obtained from the JANGLER-SNAPPER-IVY airborne gage measurements are due to the same cause that produced the high free-air peak overpressures at GREENHOUSE Easy, the explanation cannot be entirely a matter of the aerodynamics of shock reflection, but must also involve interaction between thermal radiation and blast energies in the intensely heated region at and above the surface in the neighborhood of ground zero. The significance of these high apparent reflection factors should not, however, be over-emphasized since, because of the cube root scaling law, they are very sensitive to any small systematic errors that may be present in the pressure measurements.

4.4 PATH OF THE TRIPLE POINT

The time interval, $T_2 - T_1$, between the direct and reflected shocks of Shot 4 is plotted against slant range in Fig. 4.5. The smoothed curve drawn in the figure may be interpreted as an approximation to what this interval would have been if the actual canister positions had been distributed along a correspondingly smoothed locus in space. The extrapolation of this curve to zero time interval at a slant range of 62,000 ft gives a single point on the path of the triple point at an altitude of about 18,000 ft above sea-level. Since only this one point is determined by the data, the slope of the triple point path shown in Fig. 3.1 is merely schematic. Pressure measurements on the surface and at 10 ft above the surface by Project 1.1b[8] gave no indication of the formation of a Mach stem out to a ground range of 13,250 ft.

For weak shocks, at angles of incidence slightly less than the extreme angle for regular reflections, the angle of reflection is at least equal to and in general greater than the angle of incidence. The actual distance from ground zero of the point of reflection of the reflected wave reaching the most distant canister, No. 6, cannot, therefore, be greater than that of a wave following the acoustic path (angles of incidence and reflection equal). On this basis the points of reflection for all canisters must have fallen within an arc of less than 18,000 ft radius about ground zero. Within this radius and over the sector subtended by the canister azimuths from ground zero (240° to 232° approximately), the topographic elevation varies from 4191 ft at ground zero down to about 4110 ft at the lowest estimated point of reflection and up to about 4195 ft at the limiting radius and azimuth. At no point within the possible area of reflection is the slope of the ground greater than 1° and over most of the area it is much flatter. Therefore topographic irregularity could have had little effect on the configuration of the reflected wave and the formation of the Mach stem in the direction and over the range of distances covered by the present observations. The mean elevation of the surface over the possible area

UNCLASSIFIED ~~SECRET RESTRICTED DATA~~

of reflection is about 4125 ft, giving an effective height of burst of 6088 ft, which is equivalent to 2440 ft for 1 KT at sea level.

The time interval between direct and reflected shocks for Shot 9 is plotted against slant range in Fig. 4.6. Since the canisters in the region of regular reflection were distributed around two different levels, extrapolation of the curves to zero time interval gives two points on the path of the triple point. These points, together with the conditions that the path must lie above all canisters that showed a single peaked shock, fix the position of the triple point within about ± 500 ft in horizontal distance over altitudes between 6500 ft and 10,500 ft. The inferred path is shown in Figs. 3.2 and 4.7.

Using the free-air peak overpressure function tabulated in Table A.1 and the theory of regular reflection[9] the extreme angle of incidence for regular reflection for Shot 9 is found to be 48.5° and the distance from ground zero to the limit of regular reflection is approximately 2740 ft. A circle of this radius about ground zero falls entirely within the flat floor of Frenchman Lake, so that in this case the effective reflecting surface deviates by only a matter of inches from a true horizontal plane. Using the above value of the extreme angle for regular reflection, λe, and an empirical curve based on small charge experiments[10],[11] from which the path of the triple point may be determined for a given λe, the path shown in Fig. 4.7 has been computed. Whether the indicated slower rate of rise of the triple point in the present test, as compared to that computed from the high-explosive tests, is an effect of the variation of atmospheric properties with altitude or is due to non-scaling surface reflectivity effects cannot be determined at present.

4.5 POSITIVE PHASE DURATION

The duration of the positive overpressure phase is plotted against slant range (both scaled to 1 KT in a homogeneous sea-level atmosphere) in Fig. 4.8. Points for which the measured positive phase durations are expected to be too small due to failure of the reference chambers to seal are indicated by upward pointing arrows in the figure. It will be noted that most of these values are in fact low with respect to the more reliable data.

4.6 STRENGTH OF THE REFLECTED AND MACH SHOCKS

The ratio of peak overpressure increment, ΔP_2, in the reflected shock to that in the direct free-air shock, ΔP_1, is listed in Table 4.5, along with the inverse ratio of the travel times, T_1/T_2. The choice of T_1/T_2 as a comparison variable is based on simple acoustic considerations. For an acoustic signal in a homogeneous medium, originating from a point source above a perfectly reflecting plane, the reflected wave has the same amplitude as the direct wave from a source of the same strength situated at the image point below the reflecting plane. Since the acoustic signal amplitude is inversely proportional to the distance, and the distances from the source and its image are proportional to the respective travel times, we have $\Delta P_2/\Delta P_1 = T_1/T_2$. Although in the present case we are dealing with shocks that are comparatively weak at
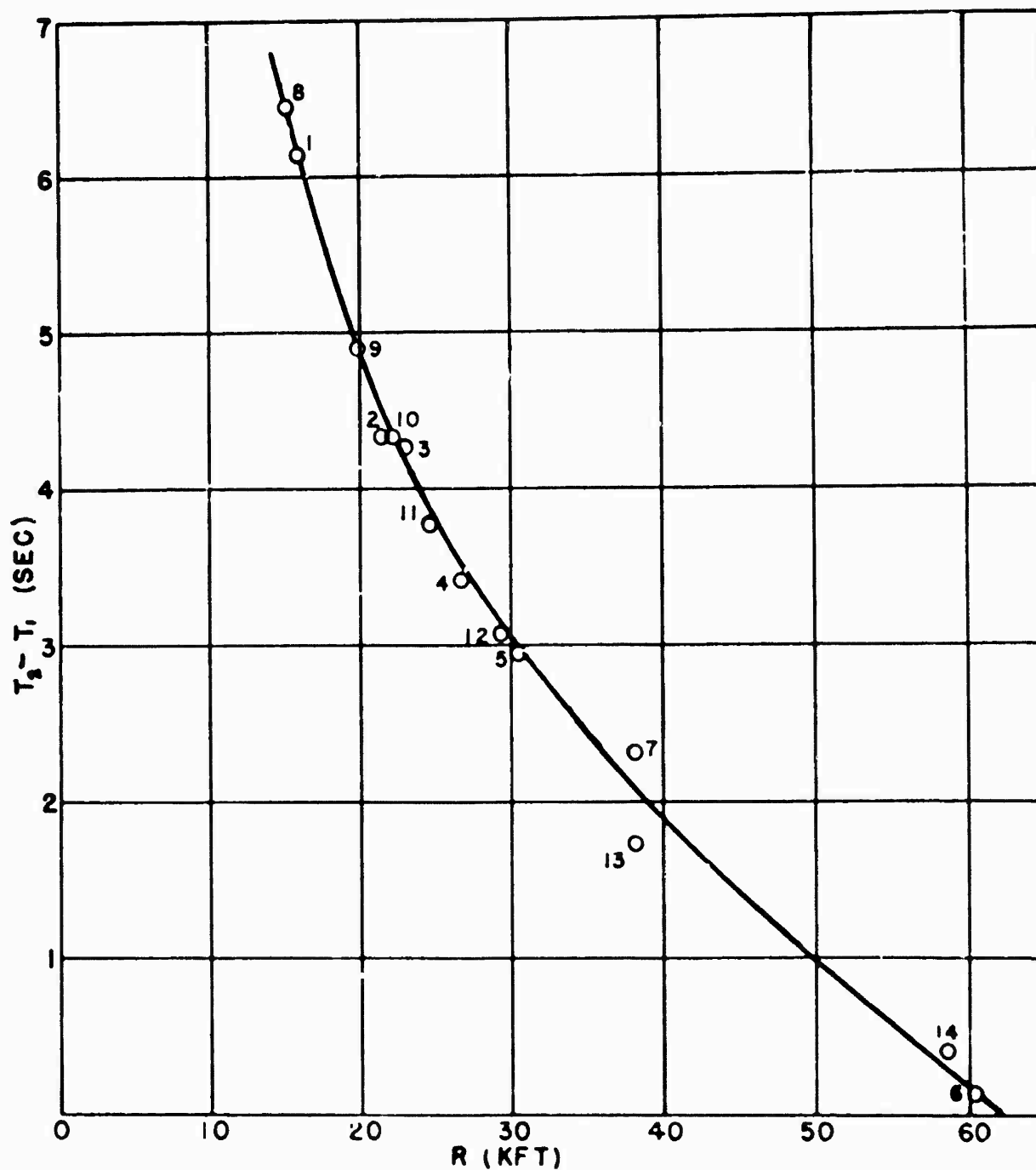
41

Fig. 4.5 Shot 4, Time Interval between Direct and Reflected
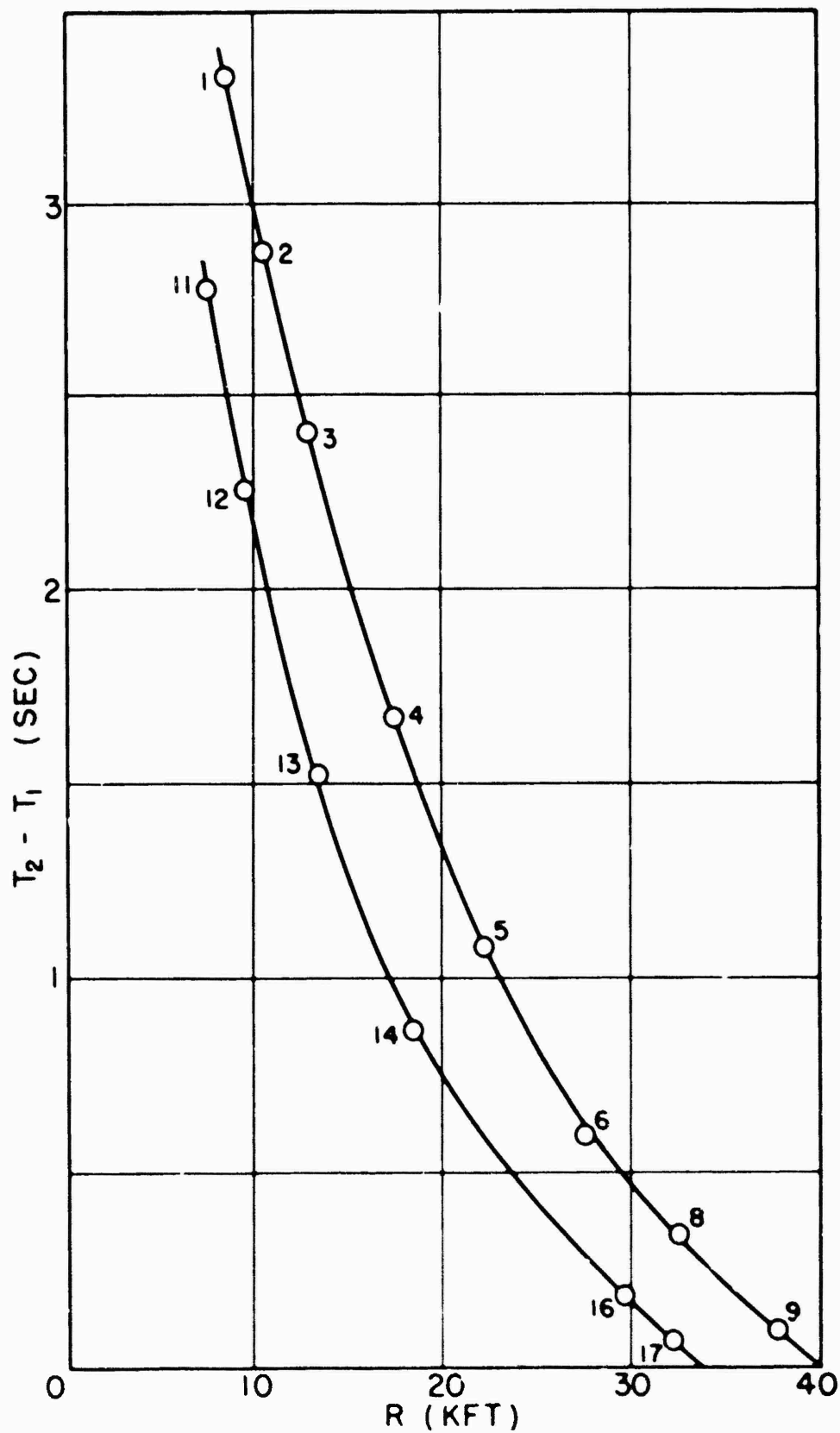Shocks vs. Slant Range

42

Fig. 4.6 Shot 9, Time Interval between Direct and Reflected Shock vs
Slant Range

43

the point of measurement, they are not weak enough to be treated acoustically at the point of reflection. Appreciable departures from the simple acoustic ratio of peak overpressures are therefore to be expected. However, the plot of $\Delta P_2/\Delta P_1$, against T_1/T_2 shown in Fig. 4.9 shows that these ratios are roughly equal for T_1/T_2 less than about 0.93 in the case of Shot 4 and less than about 0.82 for Shot 9. In each case there appears to be a marked decrease in the relative peak overpressure of the reflected shock as the triple point is approached. In the absence of a complete theory of Mach reflection we cannot generalize from these observations, but it is interesting to note that in Bargmann's (12), (13) approximate theory of Mach reflection of weak shocks at nearly glancing angles of incidence the reflected wave does not appear in the first approximation as a shock, but as a discontinuity in pressure gradient. In the second approximation there is a finite reflected shock, but the pressure increments in this shock still approach zero at the triple point. Indications of a maximum in the strength of the reflected shock at some point just above the triple point have also been noted in shock tube experiments(13).

For values of T_1/T_2 equal to or greater than 0.98, the mean value of $\Delta P_2/\Delta P_1$ is 0.46, and if this ratio is applicable right up to the triple point, the peak overpressure at the top of the Mach shock should be about 46 per cent greater than the free-air peak overpressure at the same slant range. If we make the assumption that far below the triple point the Mach overpressures are equal to the free-air overpressures from a bomb of twice the yield, the ratio of Mach to free-air peak overpressure at the same slant range should approach the value $2^{1/3} = 1.26$,
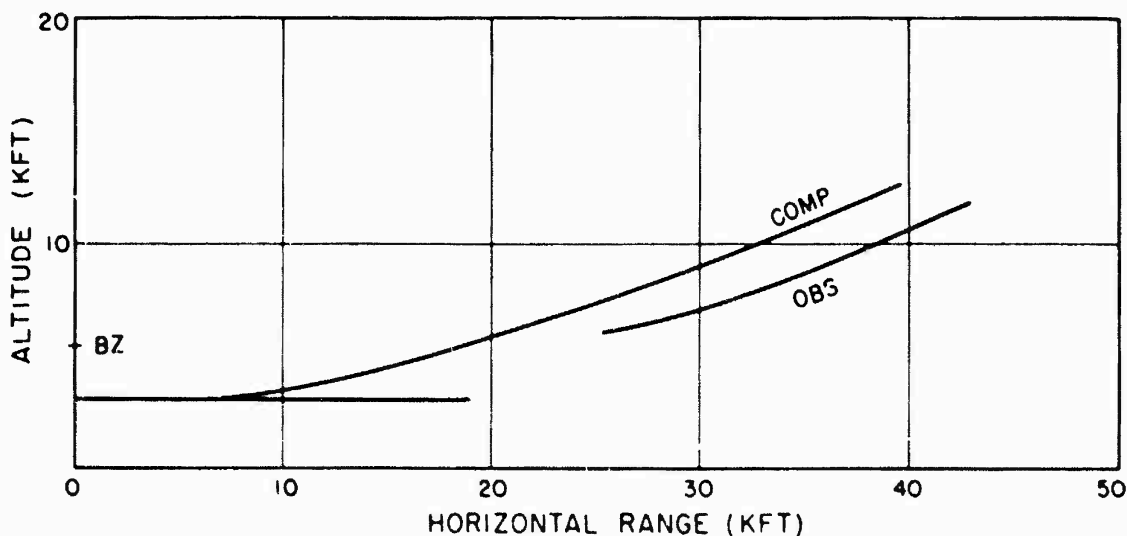

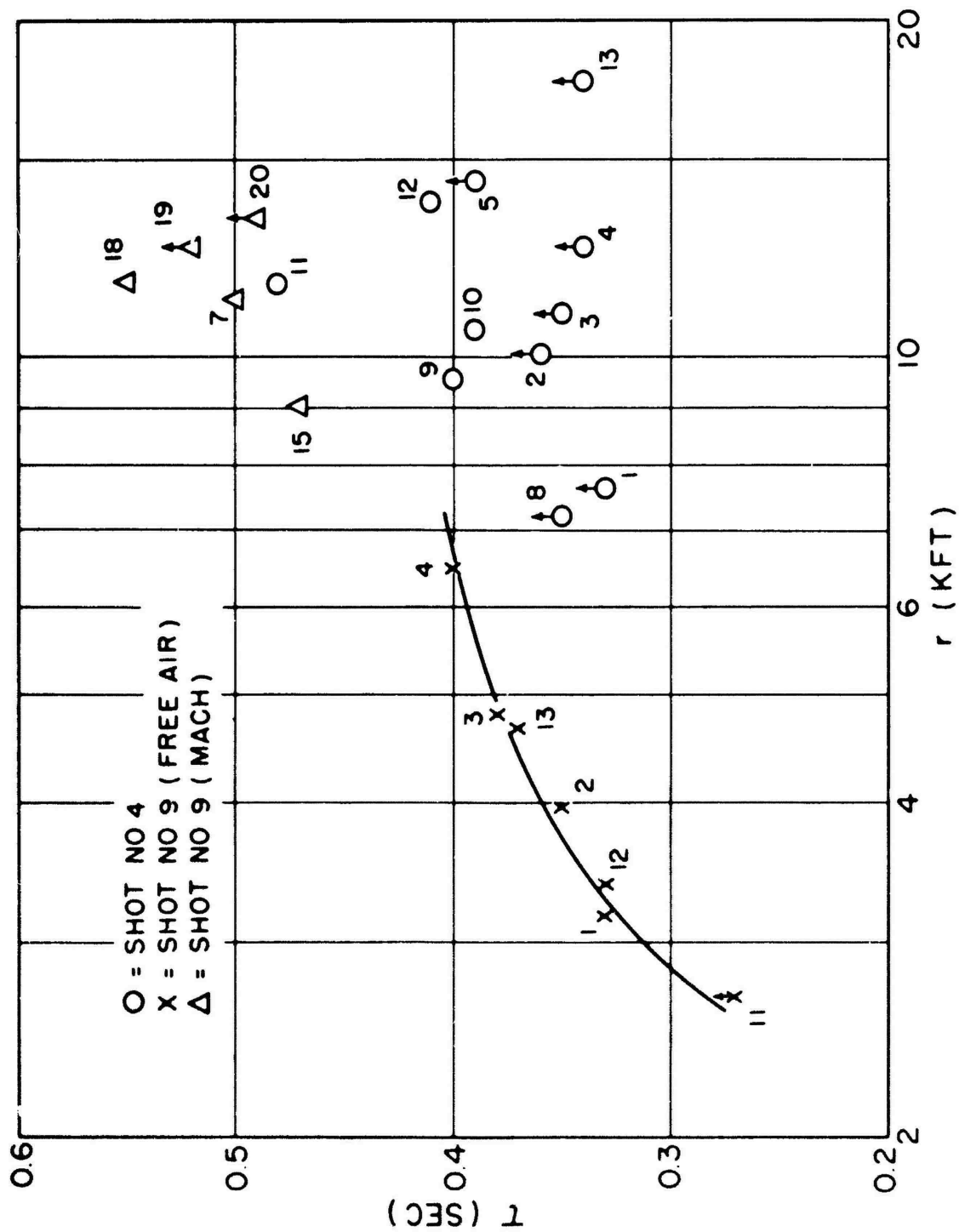Fig. 4.7 Path of the Triple Point for Shot 9 Compared with HE Scaled Path

44

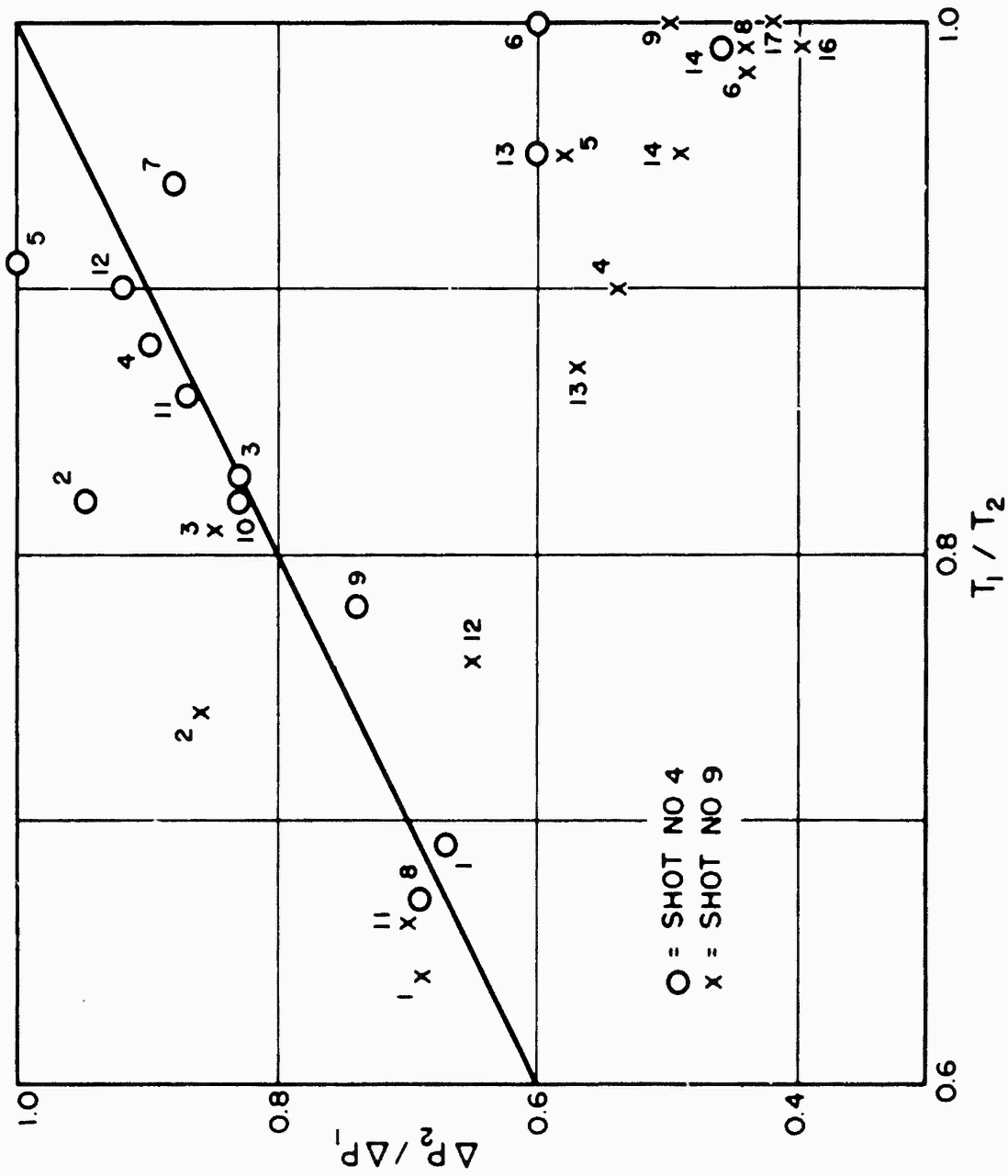Fig. 4.8 Positive Phase Duration vs Slant Range, Reduced to 1 KT at Sea-Level

45

Fig. 4.9 Ratio of Amplitudes of Direct and Reflected Shocks

O = SHOT NO 4
X = SHOT NO 9

$\Delta P_2 / \Delta P_1$

T_1 / T_2

46

TABLE 4.5 Ratio of Peak Overpressures in Direct and Reflected Shocks

Shot No. 4			Shot No. 9		
Canister No.	$\Delta P_2/\Delta P_1$	T_1/T_2	Canister No.	$\Delta P_2/\Delta P_1$	T_1/T_2
1	0.67	0.69	1	0.69	0.64
2	0.95	0.82	2	0.86	0.74
3	0.83	0.83	3	0.85	0.81
4	0.90	0.88	4	0.54	0.90
5	1.00	0.91	5	0.58	0.95
6	0.60	1.00	6	0.44	0.98
7	0.88	0.94	8	0.44	0.99
8	0.68	0.67	9	0.50	1.00
9	0.74	0.78	11	0.70	0.66
10	0.83	0.82	12	0.65	0.76
11	0.87	0.86	13	0.57	0.87
12	0.92	0.90	14	0.49	0.95
13	0.60	0.95	16	0.40	0.99
14	0.43	0.99	17	0.42	1.00

since at the low overpressures with which we are concerned the free-air peak overpressure diminishes nearly as R^{-1}. Values of $\Delta P_m/\Delta P_1$ for the canisters in the Mach region of Shot 9 are given in Table 4.6 where ΔP_1 is defined as the free-air peak overpressure at the same slant range as read from the free-air curves for this shot. It will be noted that the ratios for canisters 7, 18, 19 and 20 are very close to the value of 1.46 indicated by the reflected pressures observed above the triple point, while the ratio for canister No. 10, which is the farthest from the triple point, is not far from the "ideal" limiting value of 1.26.

4.7 THE SECONDARY SHOCK OF SHOT 9

Mention has been made previously of the very weak shocks that appear on the records of Shot 9 in addition to the main direct and reflected shocks. These shocks are small enough so that their propagation

velocity differs insignificantly from the local sound velocity. There-
fore, assuming that they originate from a weak secondary pulse emitted
from the same source as the primary shock, the arrival time of the first
should be very nearly a linear function of slant range. If the second
weak shock is the ground reflection of the first, its arrival time

TABLE 4.6 Ratio of Peak Overpressures in the Mach and Free-Air
Shocks at the Same Slant Range, Shot 9

Canister No.	P_m/P_1
7	1.48
10	1.17
15	1.63
18	1.41
19	1.42
20	1.43

should be nearly a linear function of the slant range from the image of
the source. Small departures from a linear relationship are to be
expected due to the variation of sound and wind velocity with altitude
and the fact that the secondary shocks are superimposed on the direct
and reflected primary waves. The differences between the observed
arrival times and the linear function $0.97 + R/1050$ are given in Table
4.7. For the reflected secondary (arrival time T_4) the same linear
function is used with the distance from the image source, R_1, in place
of R. From the smallness of these residuals there can be little doubt
that the above assumptions are essentially correct. The mean apparent
sound velocity between the nearest and farthest canisters, as computed
from the ambient temperature and wind data, is 1068 ft/sec. Since the
difference between this and the 1050 ft/sec that fits the weak shock
arrival times is less than the expected 2 per cent accuracy of the
slant ranges as determined from the main shock travel times, this may
be taken as confirmation of the latter.

Since the secondary shock must have traveled at appreciably higher
than ambient sound velocity in its early stages, the intercept time of
0.97 sec must be somewhat less than the actual time of origin of this
shock.

48

UNCLASSIFIED

TABLE 4.7 Time Residuals of Secondary Shock, Shot 9

Canister No.	$T_3 - (0.97 + R/1050)$	$T_4 - (.097 + R_1/1050)$
1	+0.19 (?)	
2	-0.14	+0.41
3	+0.01	
4	+0.01	
5	+0.24	
6	+0.05	+0.02
7	+0.02	-0.01
8	-0.34	-0.39
9	-0.15	-0.29
10	+0.09	-0.27 (?)
11	+0.09	+0.57
12	+0.07	
13	+0.07	+0.21
14	+0.19	+0.18
15	+0.06	0.0
16	-0.42	-0.44
17	-0.03	-0.12
18	+0.06	-0.03
19	+0.12	-0.04
20	+0.01	-0.16

CHAPTER 5

CONCLUSIONS AND RECOMMENDATIONS

5.1 NORMALIZED FREE-AIR PEAK OVERPRESSURE

The principal conclusion of the present work is represented by the normalized free-air peak overpressure curve shown in Fig. 4.4 and tabulated in Appendix, Table A.4. It is considered that further measurements of the same kind would not alter this curve substantially, but would merely provide more statistical data on which to base conclusions regarding the variability of peak overpressures. Tentative conclusions may be derived on this point from the present data. Considering all measurements from both shots, the root mean square percentage deviation from the tabulated curve is 17 per cent. However, an unduly large fraction of this comes from the large deviations of canisters 3, 4, and 14 on Shot 4. If these readings are discarded, the variance is reduced to 9.6 per cent, which is of about the same order as the apparent variance estimated from the results of previous tests with the same equipment. It is not certain how much of this is to be attributed to errors of measurement and how much is due to real variations in peak overpressure caused by variations in the effective blast output of the bomb or by the effects of small scale inhomogeneities in the atmosphere such as turbulence, wind shears, temperature fluctuations, etc.

5.2 PATH OF THE TRIPLE POINT

The disagreement between the observed path of the triple point on Shot 9 and that calculated from small charge data indicates that at present we have no means for making a reliable prediction of this path at high altitudes. Since the blast-induced loads on aircraft may be quite different on opposite sides of the path, further information is clearly desirable from the point of view of the positioning of test aircraft as well as in connection with the delivery problem for bombs of very large yield.

5.3 STRENGTH OF THE REFLECTED AND MACH SHOCKS

The occurrence just above the triple point of a maximum in the ratio

UNCLASSIFIED

of peak overpressure in the reflected shock to that in the direct shock, which is in qualitative agreement with theoretical and shock tube results, gives added weight to the need for more detailed study of the pressure distribution in the neighborhood of the triple point. The variation of time interval between direct and reflected shocks in this region is also an important factor since increased dynamic stresses on aircraft are to be expected at points where this interval coincides with a natural period of a critical structural element.

The conclusion that the peak overpressure at the triple point is about 1.46 times as great as the free-air peak overpressure and that this ratio diminishes to a limiting value of about 1.26 well below the triple point must be considered as very tentative, since it rests on relatively few measurements and a single height of burst. It should also be emphasized that these ratios are applicable only at low overpressures (say less than 2 psi) and at points far above the reflecting surface.

The time and expenditure needed to obtain detailed data on the path of the triple point at high altitudes, and the distribution of overpressures in its neighborhood, would be prohibitive if it were to be done directly with airborne pressure gages and atomic detonations at a wide range of heights of burst. It is therefore recommended that the available small charge data be checked and extended as a preliminary step. Although, as indicated by the present results, it is not expected that the HE data will scale quantitatively, only a few full-scale atomic tests may be necessary to indicate how the HE curves must be modified for use in predicting the corresponding effects for atomic bombs.

With the present telemetering canister instrumentation there are severe limitations on the amount of data than can be obtained on any one shot. Considering the uncertainty in the preshot estimate of the position of the triple point trajectory and the possibility of large errors in the deployment of the canisters at pre-assigned positions and times with respect to an air-burst bomb it must be considered as unusually fortunate that the present test yielded as much data as it did. For future measurements in the neighborhood of the triple point it is recommended that consideration be given to the development of a very small parachute-borne canister, with a self contained pressure recording system that could be deployed in large numbers and subsequently recovered. For tests conducted at the Nevada Proving Grounds a high percentage of recovery may be anticipated. In the UPSHOT-KNOTHOLE tests 30 canisters were recovered out of 34 dropped, in most cases with no damage beyond a bent pressure probe.

UNCLASSIFIED

APPENDIX A

METEOROLOGICAL DATA

TABLE A.1 - Shot 4 Radiosonde Data for 6 April 1953, 1530 Z (=0730 PST)

Altitude (k ft)	Pressure (psi)	Temperature (°C)	Sound Velocity (ft/sec)	Wind Velocity (ft/sec)	Wind Direction
4.025	12.49	15.5	1117	12	045
5	12.10	12.0	1111	3	030
6	11.69	9.1	1106	5	300
7	11.26	5.7	1098	17	310
8	10.79	3.6	1094	22	310
9	10.44	1.9	1091	35	280
10	10.07	0.0	1087	47	280
11	9.66	-2.3	1083	52	280
12	9.31	-4.0	1079	56	280
13	8.96	-6.4	1075	76	280
14	8.62	-8.8	1070	81	280
15	8.33	-10.8	1066	52	280
16	7.99	-13.1	1061	57	280
17	7.66	-14.5	1058	63	280
18	7.34	-15.7	1056	108	290
19	7.05	-17.9	1051	123	290
20	6.79	-20.1	1047	122	290

52

TABLE A.2 - Shot 9 Radiosonde Data for 8 May 1953, 1530 Z (=0730 PST)

Altitude (k ft)	Pressure (psi)	Temperature (°C)	Sound Velocity (ft/sec)	Wind Velocity (ft/sec)	Wind Direction
5.5	12.23	+8.0	1103	12	255
6	11.96	+6.7	1100	13	270
7	11.48	+4.2	1095	15	295
8	11.02	+1.2	1090	17	320
9	10.58	-1.0	1086	17	300
10	10.16	-3.0	1081	20	260
11	9.77	-5.0	1077	32	255
12	9.43	-6.0	1075	44	250

53

TABLE A.3 - Altitude Scale Factors

Altitude (k ft)	Shot 4		Shot 9	
	λ	μ	λ	μ
4	0.869	0.955		
5	0.890	0.965		
5.5			1.000	1.000
6	0.911	0.974	1.015	1.005
7	0.932	0.981	1.045	1.016
8	0.953	0.983	1.075	1.026
9	0.975	0.991	1.107	1.038
10	1.000	1.000	1.139	1.049
11	1.026	1.007	1.173	1.060
12	1.054	1.017	1.207	1.073
13	1.082	1.027		
14	1.111	1.035		
15	1.141	1.047		
16	1.173	1.058		
17	1.205	1.065		
18	1.240	1.075		
19	1.275	1.085		
20	1.312	1.098		

TABLE A.4 — Normalized Composite Free-Air Peak Overpressure Function, $f(r)$

r (ft)	0	1	2	3	4	5	6	7	8	9	10
150	633	617	602	588	575	562	550	538	527	516	505
160	505	494	484	474	464	454	445	436	427	418	410
170	410	402	395	388	381	374	368	362	356	350	344
180	344	338	333	328	323	318	313	308	303	299	295
190	295	291	287	283	279	275	271	267	263	259	256

r (ft)	0	10	20	30	40	50	60	70	80	90	100
200	256	227	202	180	161	144	129	116	105	96	88
300	88.0	80.4	73.9	68.3	63.5	59.3	55.7	52.5	49.6	47.0	44.6
400	44.6	42.3	40.1	38.0	36.1	34.4	32.8	31.3	29.9	28.6	27.4
500	27.4	26.3	25.3	24.4	23.5	22.7	21.9	21.2	20.5	19.9	19.3
600	19.3	18.7	18.1	17.6	17.1	16.6	16.1	15.6	15.1	14.7	14.3
700	14.3	13.9	13.5	13.1	12.8	12.5	12.2	11.9	11.6	11.3	11.1
800	11.10	10.85	10.61	10.38	10.15	9.93	9.72	9.51	9.30	9.10	8.90
900	8.90	8.71	8.53	8.36	8.20	805	7.90	7.76	7.63	7.51	7.40
1000	7.40	7.29	7.18	7.07	6.96	6.85	6.75	6.65	6.55	6.45	6.35

TABLE A.4 (Continued)

r (ft)	0	10	20	30	40	50	60	70	80	90	100
1100	6.35	6.26	6.17	6.08	6.00	5.92	5.84	5.76	5.68	5.60	5.52
1200	5.52	5.45	5.38	5.31	5.24	5.17	5.10	5.03	4.97	4.91	4.85
1300	4.85	4.79	4.73	4.67	4.61	4.55	4.50	4.45	4.40	4.35	4.30
1400	4.30	4.25	4.20	4.15	4.10	4.05	4.01	3.97	3.93	3.89	3.85
1500	3.85	3.81	3.77	3.73	3.69	3.65	3.61	3.58	3.54	3.50	3.47
1600	3.47	3.44	3.41	3.37	3.34	3.30	3.27	3.24	3.21	3.18	3.15
1700	3.15	3.12	3.09	3.06	3.03	3.00	2.98	2.95	2.93	2.90	2.88
1800	2.88	2.85	2.83	2.80	2.78	2.75	2.73	2.71	2.69	2.67	2.65
1900	2.65	2.63	2.61	2.59	2.57	2.55	2.53	2.51	2.49	2.47	2.45

r (ft)	0	100	200	300	400	500	600	700	800	900	1000
2000	2.45	2.28	2.13	2.00	1.88	1.77	1.67	1.58	1.49	1.41	1.33
3000	1.330	1.259	1.195	1.137	1.085	1.039	.998	.961	.923	.898	.870
4000	.870	.843	.817	.791	.766	.741	.717	.694	.672	.651	.630
5000	.630	.610	.592	.575	.559	.544	.530	.517	.505	.494	.484
6000	.484	.473	.463	.453	.443	.434	.425	.416	.408	.400	.393
7000	.393	.386	.379	.372	.365	.359	.353	.347	.341	.335	.329

56

r (ft)	0	100	200	300	400	500	600	700	800	900	1000
8000	.329	.324	.319	.314	.309	.304	.299	.295	.290	.286	.282
9000	.282	.278	.274	.270	.266	.262	.259	.255	.252	.249	.246
	0	1000	2000	3000	4000	5000	6000	7000	8000	9000	10,000
10,000	.246	.221	.199	.180	.164	.151	.141	.132	.124	.116	.109
20,000	.109	.1021	.0963	.0914	.0873	.0838	.0805	.0773	.0742	.0712	.0684
30,000	.0684	.0658	.0634	.0611	.0590	.0570	.0551	.0533	.0516	.0500	.0485
40,000	.0485	.0471	.0458	.0446	.0434	.0423	.0412	.0402	.0392	.0382	.0372

BIBLIOGRAPHY

1. N. A. Haskell and J. O. Vann, _The Measurement of Free-Air Atomic Blast Pressures_, Operation JANGLE, Project 1.3, AFSWP Report WT-367, (April 1952).

2. N. A. Haskell and J. O. Vann, _The Measurement of Free-Air Atomic Blast Pressures_, Operation SNAPPER, Project 1.1, AFSWP Report WT-511, (February 1953).

3. N. A. Haskell, J. O. Vann, and P. R. Gast, _Free-Air Atomic Blast Pressure and Thermal Measurements_, Operation IVY, Project 6.11, AFSWP Report WT-631 (August 1953)

4. K. Fuchs, _The Effect of Altitude_, Los Alamos Technical Series LA-1021, Vol VII, Pt II, Chapter 9.

5. R. G. Sachs, _The Dependance of Blast on Ambient Temperature and Pressure_, Ballistic Research Laboratories, Aberdeen Proving Ground, Report No. 466 (May 1944).

6. C. J. Aronson, J. F. Moulton, Jr., J. Petes, E. J. Cullings, and E. R. Walthall, _Free-Air and Ground-Level Pressure Measurements_, Operation TUMBLER, Projects 1.3 and 1.5, AFSWP Report WT-513, (November 1952).

7. G. K. Hartmann, C. W. Lampson, and C. J. Aronson, _Blast Measurements, Summary Report_, Operation GREENHOUSE, Scientific Director's Report, Annex 1.6, WT-64 (May 1952).

8. L. M. Swift and D. G. Sachs, _Air Pressure Vs. Time_, Operation UPSHOT-KNOTHOLE, Project 1.1b, WT-711.

9. H. Polachek and R. J. Seeger, _Regular Reflections of Shocks in Ideal Gases_, BuOrd Explosives Research Report No. 13, (February 1944).

10. R. R. Halverson, _The Effect of Air Burst on the Blast from Bombs and Small Charges_, II., Analysis of Experimental Results, OSRD Report No. 4899, (April 1945).

11. Summary Technical Report of Division 2, NDRC, _Effects of Impact and Explosion_, (1946).

12. V. Bargmann, _On Nearly Glancing Reflection of Shocks_, AMP Report 108.2R, NDRC (1945).

13. C. H. Fletcher, A. H. Taub, and W. Bleakney, _The Mach Reflection of Shocks at Nearly Glancing Incidence_, Rev. Mod. Phys 23, 271 (1951).

58

UNCLASSIFIED SE

DISTRIBUTION

Military Distribution Category 5-21

93 Officer-in-Charge, U.S. Naval Civil Engineering Res. and Evaluation Lab., U.S. Naval Construction Battalion Center, Port Hueneme, Calif. ATTN: Code 753

94 Commanding Officer, U.S. Naval Medical Research Inst., National Naval Medical Center, Bethesda 14, Md.

95 Director, U.S. Naval Research Laboratory, Washington 25, D.C. ATTN: Code 2029

96 Commanding Officer and Director, U.S. Navy Electronics Laboratory, San Diego 52, Calif. ATTN: Code 4223

97-98 Commanding Officer, U.S. Naval Radiological Defense Laboratory, San Francisco 24, Calif. ATTN: Technical Information Division

99-100 Commanding Officer and Director, David W. Taylor Model Basin, Washington 7, D.C. ATTN: Library

101 Commander, U.S. Naval Air Development Center, Johnsville, Pa.

102 Director, Office of Naval Research Branch Office, 1000 Geary St., San Francisco, Calif.

103-109 Technical Information Service, Oak Ridge, Tenn. (Surplus)

AIR FORCE ACTIVITIES

110 Asst. for Atomic Energy, Headquarters, USAF, Washington 25, D.C. ATTN: DCS/O

111 Director of Operations, Headquarters, USAF, Washington 25, D.C. ATTN: Operations Analysis

112 Director of Plans, Headquarters, USAF, Washington 25, D.C. ATTN: War Plans Div.

113 Director of Research and Development, Headquarters, USAF, Washington 25, D.C. ATTN: Combat Components Div.

114-115 Director of Intelligence, Headquarters, USAF, Washington 25, D.C. ATTN: AFOIN-1B2

116 The Surgeon General, Headquarters, USAF, Washington 25, D.C. ATTN: Bio. Def. Br., Pre. Med. Div.

117 Deputy Chief of Staff, Intelligence, Headquarters, U.S. Air Forces Europe, APO 633, c/o PM, New York, N.Y. ATTN: Directorate of Air Targets

118 Commander, 497th Reconnaissance Technical Squadron (Augmented), APO 633, c/o PM, New York, N.Y.

119 Commander, Far East Air Forces, APO 925, c/o PM, San Francisco, Calif.

120 Commander, Strategic Air Command, Offutt Air Force Base, Omaha, Nebraska. ATTN: Special Weapons Branch, Inspection Div., Inspector General

121 Commander, Tactical Air Command, Langley AFB, Va. ATTN: Documents Security Branch

122 Commander, Air Defense Command, Ent AFB, Colo.

123-124 Commander, Air Materiel Command, Wright-Patterson AFB, Dayton, O. ATTN: MCAIDS

125 Commander, Air Training Command, Scott AFB, Belleville, Ill. ATTN: DCS/O GTP

126 Commander, Air Research and Development Command, PO Box 1395, Baltimore, Md. ATTN: RDDN

127 Commander, Air Proving Ground Command, Eglin AFB, Fla. ATTN: AG/TRB

128-129 Commander, Air University, Maxwell AFB, Ala.

130-137 Commander, Flying Training Air Force, Waco, Tex. ATTN: Director of Observer Training

138 Commander, Crew Training Air Force, Randolph Field, Tex. ATTN: 2TTS, DCS/O

139 Commander, Headquarters, Technical Training Air Force, Gulfport, Miss. ATTN: TA&D

140-141 Commandant, Air Force School of Aviation Medicine, Randolph AFB, Tex.

142-147 Commander, Wright Air Development Center, Wright-Patterson AFB, Dayton, O. ATTN: WCOESP

148-149 Commander, Air Force Cambridge Research Center, 230 Albany Street, Cambridge 39, Mass. ATTN: CRQST-2

150-152 Commander, Air Force Special Weapons Center, Kirtland AFB, N. Mex. ATTN: Library

153 Commandant, USAF Institute of Technology, Wright-Patterson AFB, Dayton, O. ATTN: Resident College

154 Commander, Lowry AFB, Denver, Colo. ATTN: Department of Armament Training

155 Commander, 1009th Special Weapons Squadron, Headquarters, USAF, Washington 25, D.C.

156-157 The RAND Corporation, 1700 Main Street, Santa Monica, Calif. ATTN: Nuclear Energy Division

158-164 Technical Information Service, Oak Ridge, Tenn. (Surplus)

OTHER DEPARTMENT OF DEFENSE ACTIVITIES

165 Asst. Secretary of Defense, Research and Development, D/D, Washington 25, D.C.

166 U.S. National Military Representative, Headquarters, SHAPE, APO 55, c/o PM, New York, N.Y. ATTN: Col. J. P. Healy

167 Director, Weapons Systems Evaluation Group, OSD, Rm 2E1006, Pentagon, Washington 25, D.C.

168 Armed Services Explosives Safety Board, D/D, Building T-7, Gravelly Point, Washington 25, D.C.

169 Commandant, Armed Forces Staff College, Norfolk 11, Va. ATTN: Secretary

170-175 Commanding General, Field Command, Armed Forces Special Weapons Project, PO Box 5100, Albuquerque, N. Mex.

176-177 Commanding General, Field Command, Armed Forces, Special Weapons Project, PO Box 5100, Albuquerque, N. Mex. ATTN: Technical Training Group

178-186 Chief, Armed Forces Special Weapons Project, Washington 25, D.C.

187-193 Technical Information Service, Oak Ridge, Tenn. (Surplus)

ATOMIC ENERGY COMMISSION ACTIVITIES

194-196 U.S. Atomic Energy Commission, Classified Technical Library, 1901 Constitution Ave., Washington 25, D.C. ATTN: Mrs. J. M. O'Leary (For DMA)

197-199 Los Alamos Scientific Laboratory, Report Library, PO Box 1663, Los Alamos, N. Mex. ATTN: Helen Redman

200-211 Sandia Corporation, Classified Document Division, Sandia Base, Albuquerque, N. Mex. ATTN: Martin Lucero

212-213 University of California Radiation Laboratory, PO Box 808, Livermore, Calif. ATTN: Margaret Edlund

214 Weapon Data Section, Technical Information Service, Oak Ridge, Tenn.

215-225 Technical Information Service, Oak Ridge, Tenn. (Surplus)